RESEARCH ARTICLE • OPEN ACCESS

Fractional-Order COVID-19 Model in Indonesia with Comorbidity and Immunization: PID Control, Ulam-Hyers Stability, and Biosecurity Implications

Muhammad Farman *et al.*

Volume 6, Issue 4, Pages 293–310, December 2025

Received 20 August 2025, Revised 19 October 2025, Accepted 3 November 2025, Published Online 2 December 2025

To Cite this Article : M. Farman *et al.*,"Fractional-Order COVID-19 Model in Indonesia with Comorbidity and Immunization: PID Control, Ulam-Hyers Stability, and Biosecurity Implications", *Jambura J. Biomath*, vol. 6, no. 4, pp. 293–310, 2025, *https://doi.org/10.37905/jjbm.v6i4.34027*

JOURNAL INFO • JAMBURA JOURNAL OF BIOMATHEMATICS

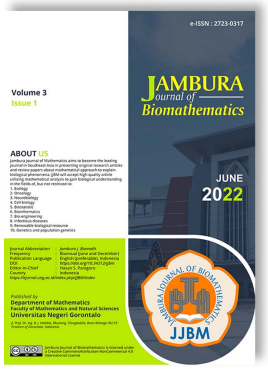

Homepage	:	http://ejurnal.ung.ac.id/index.php/JJBM/index
Journal Abbreviation	:	Jambura J. Biomath.
Frequency	:	Quarterly (March, June, September and December)
Publication Language	:	English
DOI	:	https://doi.org/10.37905/jjbm
Online ISSN	:	2723-0317
Editor-in-Chief	:	Hasan S. Panigoro
Publisher	:	Department of Mathematics, Universitas Negeri Gorontalo
Country	:	Indonesia
OAI Address	:	http://ejurnal.ung.ac.id/index.php/jjbm/oai
Google Scholar ID	:	XzYgeKQAAAAJ
Email	:	editorial.jjbm@ung.ac.id

JAMBURA JOURNAL • FIND OUR OTHER JOURNALS

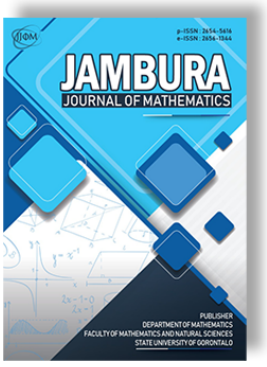

Jambura Journal of Mathematics

Jambura Journal of Mathematics Education

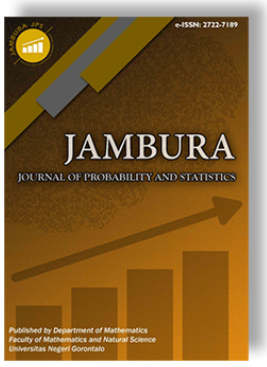

Jambura Journal of Probability and Statistics

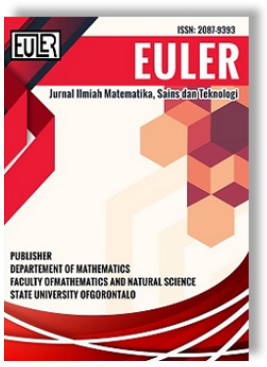

EULER : Jurnal Ilmiah Matematika, Sains, dan Teknologi

Jambura Journal of Biomathematics, Volume 6, Issue 4, Pages 293–310, December 2025 https://doi.org/10.37905/jjbm.v6i4.34027

Research Article

Check for updates

Fractional-Order COVID-19 Model in Indonesia with Comorbidity and Immunization: PID Control, Ulam-Hyers Stability, and Biosecurity Implications

Muhammad Farman[1,2], **Cicik Alfiniyah**[3,*], **Fatmawati**[3], **Muhammad Abdurrahman Rois**[4], **and Khadija Jamil**[5]

[1]*Faculty of Arts and Science, Department of Mathematics, Near East University, 99138 Nicosia, Cyprus*
[2]*Research Center of Applied Mathematics, Khazar University, Baku, Azerbaijan*
[3]*Department of Mathematics, Faculty of Science and Technology, Universitas Airlangga, Surabaya, Indonesia*
[4]*Department of Mathematics, Universitas Islam Negeri Salatiga, Salatiga, Indonesia*
[5]*Institute of mathematics, khawaja fareed university of information and technology, Raheem yar Khan Pakistan*

ARTICLE HISTORY
Received 20 August 2025
Revised 19 October 2025
Accepted 3 November 2025
Published 2 December 2025

KEYWORDS
Covid-19 model
Ulam-Hyers Stability
PID control
Fractal fractional operator
Mittag-Leffer kernel
Newton polynomial

ABSTRACT. *In this paper, we developed a fractal fractional model for Covid-19 dynamics in Indonesia with comorbidity and various immunization stages doses is presented and examined. The system is analysed disease-free according to reproductive number. We conducted both qualitative and quantitative research on the COVID-19 model using the Atangana-Baleanu fractal-fractional operator. We demonstrated the existence and uniqueness of the model with the Atangana-Baleanue fractal-fractional operator as continuous and compact integral components, by means of Krasnoselskii fixed point theorem. We ensure that our proposed model has a unique fixed-point solution by including the properties of both the Schauder and Krasnoselskii theorems into the contraction mapping. We conduct a thorough examination of the suggested model's stability using the Ulam-Hyers stability concept. We discuss how the Proportional Integral Derivative (PID) impact in a fractional COVID-19 model improves stability. Since these control methods have a great potential to improve overall treatment outcomes, minimise side effects, and correctly regulate these treatments to achieve this goal, their use will stabilise the dynamics behaviour while accurately regulating the administration, leading to better vaccination outcomes with fewer adverse effects inferred from this. A numerical approach based on Lagrange interpolation is presented. The dynamics of disease transmission throughout a range of fractional-order ϖ and fractal dimensions ϑ are then visually represented by the numerical results that have been obtained. The findings demonstrate the deep impact of fractional dynamics and fractal dimensions on the processes of vaccination, recovery, and propagation, exposing intricate, time-dependent epidemic characteristics.*

1. Introduction

COVID-19 was the disease that spread throughout the world. It showed up first in Wuhan, China, wet market after a bat transferred it to humans. The symptoms of COVID-19 are very diverse and can target different aspects like tiredness, dry cough, fever, etc. Unlike these other symptoms, sore throat, body ache pain diarrhea conjunctivitis headache rashes pale or purple toes and fingers may seem strange to many people. Warning signs include breathing difficulties or shortness of breath as well as pressure or pain in the chest area. This is contagious when people are near each other and touch one another by sneezing, coughing, sneezing or exchanging their respiratory substances. Wear mask all times while in public places keep your hands clean and maintain six feet distance from strangers are three most important preventive measures that you can do to safeguard yourself from Covid-19 infection. A lot of companies started developing vaccines as quickly as possible so far we have fifteen different types of COVID-19 vaccine available in this time period only today or now as Johnson, Oxford-AstraZeneca, Pfizer-BioNTech, Sputnik V and Moderna are some popular ones among them.

According to information taken from the web [1], Indonesia was 18th out of 222 countries in terms of COVID-19 infections recorded as of June 14, 2021. 1,919,547 cases were confirmed nationwide, resulting in 1,751,234 recoveries and 53,116 deaths. To control the rising number of COVID-19 infections and stop the outbreak, a successful plan is required. The World Health Organization (WHO) drew up plans aimed at halting the spread of COVID-19, which included mandating masks in public spaces, social distancing, hospital or other purpose-built isolation areas were to be established, and stringent rules for contact tracing applied [2]. Public education is critical in terms of informing people about what they can do to keep themselves and others safe from the virus to ensure COVID-19 doesn't spread. Vaccination is a fundamental method for preventing significant harmful effects on public health as well during the emergence of new viral

*Corresponding Author.
Email : *cicik-a@fst.unair.ac.id* (C. Alfiniyah)
Homepage : http://ejurnal.ung.ac.id/index.php/JJBM/index / E-ISSN : 2723-0317

agents such as COVID-19 [3, 4]. The first immunization against COVID-19 illness started in Indonesia at the start of 2021. Additionally, booster shots are crucial for establishing immunity in the body following the second vaccination because they have been shown to lower the death rate and worst-case hazards associated with COVID-19 by up to 91% [5]. Early in 2022, a circular on the three-dose or booster vaccine necessary to maintain immunity against COVID-19 infection was released by the Indonesian Ministry of Health through the Directorate General of Disease Prevention and Control. Moreover, mathematicians are expending much labor in the search for a resolution to this issue. We need to know how fast a disease could spread, so the use of mathematical models will allow us not only forecast but control and plan measures ahead such as lockdowns or social distancing with adequate strategies reduce the impact.

Fractional order techniques, in addition to conventional derivatives, are useful for extremely perceptive issue interpretation [6, 7]. The fundamental idea of fractional derivatives, which was based on the law of power, was established by Riemann-Liouville. Atangana and Alkahtani presented the most recent method, the fractional derivative, in [8]. A non-singular kernel with an updated fractional derivative including trigonometric and exponential functions has been proposed in previous research [9], and [10] describes numerous novel strategies for disease models. For this new operator, necessary effects have been built, and Khan et al. [11] provides illustrations. Applying a standard approach to the mode's method, the problem is analyzed and numerical solutions are obtained in [12]. A mathematical model utilizing the Mittag-Leffler function to investigate the stability and intricate dynamics of COVID-19 dissemination is presented in [13]. The study [14] uses a mathematical model based on a fractal fractional operator to examine the relationship between diabetes mellitus and COVID-19. They give a thorough examination of the co-infection dynamics, providing information on how these conditions affect patient outcomes. The article [15] investigates the application of fractal-fractional operators to create a mathematical model of COVID-19 spread that is more precise. A thorough analysis of fractional order model construction and implementation in epidemic modeling [16]. It highlights the significance of these models in comprehending complex biological systems and disease dynamics by going over their evolution, current applicability in the life sciences, and possible future possibilities. A new fractal-fractional model for controlling tuberculosis prevalence [17]. It evaluates the sensitivity and stability of the model and contains simulations to test its efficacy in real-world scenarios, offering insights into possible tuberculosis control techniques. In numerous works, the field of mathematical biology uses various formulas for classical and fractional operators to understand the dynamics of disease transmission and spread. But fractal fractional operators are still underutilized, particularly when it comes to the dynamics of COVID-19 pandemic diseases. For this reason, the study presented in this paper relies significantly on this source of information. Here, we structure a model related to COVID-19 and use the fractal fractional Mittag-Leffler kernel operation to mathematical epidemiology. The aim of this study is to explore the dynamic behavior of COVID-19 by using a fractional-fractional Mittag-Leffler kernel operator to expand the epidemiological model, as inspired by [5].

In order to analyze Covid-19 model, this study presents a unique model that combines fractional calculus and fractals with the Mittag-Leffler kernel. The article is set up like this: An overview of the aims and objectives of the study is given in Section 1. The operators utilized in the analysis are defined in Section 2. In Section 3, a mathematical model for investigating Covid-19 model is presented that combines the Mittag-Leffler kernel with fractional and fractal. A thorough examination of the suggested model is provided in Section 4. Ulam-Hyers evaluates the system's stability in Section 5. PID control's applicability is examined in Section 6. The model numerical scheme, which are presented in Section 7. The results are compiled and the final conclusions are presented in Section 8,9.

2. Basic Concepts

Here, we provide some essential definitions that could help with system analysis.

Definition 1. [18] Assume that $\beth_1(t)$ is continuous within the interval (a, b) and has fractal differentiability of order ϖ. Then, when $0 \leq \varpi, \upsilon \leq 1$, the fractal-fractional derivative with order ϖ can be represented using the Riemann-Liouville derivative.

$$ {}_0^{FFP}\mathrm{D}_t^{\varpi,\vartheta}\beth_1(t) = \frac{1}{\Gamma(n-\varpi)}\frac{d}{dt^{\vartheta}}\int_0^t (t-\varsigma)^{n-\varpi-1}\beth_1(\varsigma)d\varsigma, \tag{1} $$

where $n-1 < \varpi, \vartheta < n \in \mathfrak{N}$, and $\frac{\mathrm{D}\beth_1(\varsigma)}{\mathrm{D}\varsigma^{\vartheta}} = \lim_{t\to\varsigma}\frac{\beth_1(t)-\beth_1(\varsigma)}{t^{\varpi}-\varsigma^{\vartheta}}$.

$$ {}_0^{FFE}\mathrm{D}_t^{\varpi,\vartheta}\beth_1(t) = \frac{\mathcal{Q}(\varpi)}{\Gamma(n-\varpi)}\frac{d}{dt^{\vartheta}}\int_0^t \exp\Big[-\frac{\varpi}{1-\varpi}(t-\varsigma)\Big]\beth_1(\varsigma)d\varsigma, \tag{2} $$

where $\varpi > 0$, $\vartheta \leq n \in \mathfrak{N}$, and $\mathcal{Q}(0) = 1 = \mathcal{Q}(1)$.

$$ {}_0^{FFM}\mathrm{D}_t^{\varpi,\vartheta}\beth_1(t) = \frac{\mathcal{AB}(\varpi)}{1-\varpi}\frac{d}{dt^{\vartheta}}\int_0^t \beth_1(\varsigma)W_{\varpi}\Big[-\frac{\varpi}{1-\varpi}(t-\varsigma)^{\varpi}\Big]d\varsigma. \tag{3} $$

Here, $0 < \varpi, \vartheta \leq 1$, W_{ϖ} represents the Mittag-Leffler function, and $\mathcal{AB}(\varpi) = 1-\varpi+\frac{\varpi}{\Gamma(\varpi)}$ denotes a normalization function.

Definition 2. [18] If $\beth_1(t)$ to be continuous on (a, b) and $0 \leq \varpi, \vartheta \leq 1$, $\beth_1(t)$ has a fractal dimension of ϑ and a fractional order of φ.

$$ {}_0^{FFP}\mathrm{I}^{\varpi,\vartheta}\beth_1(t) = \frac{1}{\Gamma(\varpi)}\int_0^t (t-\varsigma)^{\varpi-1}\varsigma^{1-\vartheta}\beth_1(\varsigma)d\varsigma. \tag{4} $$

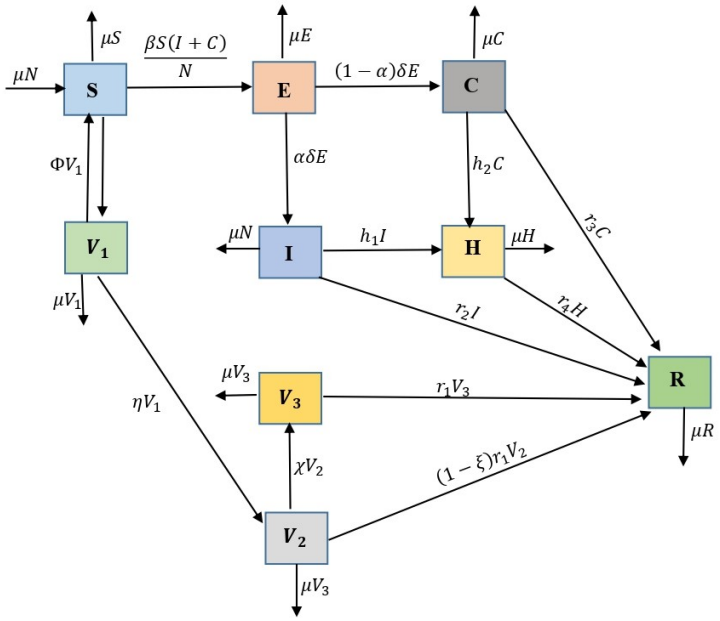

Figure 1. Flow Diagram of the Covid-19 Model

$$ {}_{0}^{FFE}\mathrm{I}^{\varpi,\vartheta}\rbrack_1(t) = \frac{\vartheta(1-\varpi)t^{\vartheta-1}\rbrack_1(t)}{\mathcal{Q}(\varpi)} + \frac{\varpi\vartheta}{\mathcal{Q}(\wp)}\int_0^t \varsigma^{\varpi-1}\rbrack_1(\varsigma)d\varsigma. \tag{5} $$

$$ {}_{0}^{FFM}\mathrm{I}^{\varpi,\vartheta}\rbrack_1(t) = \frac{\varpi\vartheta}{\mathcal{AB}(\varpi)\Gamma(\varpi)}\int_0^t (t-\varsigma)^{\varpi-1}\varsigma^{\vartheta-1}\rbrack_1(\varsigma) + \frac{\vartheta(1-\vartheta)t^{\varpi-1}\rbrack_1(t)}{\mathcal{AB}(\varpi)}d\varsigma. \tag{6} $$

3. Formulation of Model

Table 1. Covid-19 model parameters.

Parameter	Description
β^{ϖ}	The rate of infection contact
μ^{ϖ}	The rate of natural births or deaths
Λ^{ϖ}	The initial vaccination dose rate
Φ^{ϖ}	Rate of progression from V_1 to S
η^{ϖ}	The second vaccination dose rate
χ^{ϖ}	The third vaccine dose rate
r_1^{ϖ}	The rate of recovery for the V2/V3 population
r_2^{ϖ}	I population recovery rate
r_3^{ϖ}	C population recovery rate
r_4^{ϖ}	H population recovery rate
ξ^{ϖ}	Percentage of the V_2 population that had a full recovery
δ^{ϖ}	Rate of movement within the E population
α^{ϖ}	Percentage of E that spreads disease
h_1^{ϖ}	Rate of I population isolation
h_2^{ϖ}	Rate of C population isolation

This model [5] divides the total population N of humans into susceptible S, vaccinated V_1, vaccinated V_2, vaccinated V_3, exposed E, infected without comorbidity I, infected with comorbidity C, isolated H, and recovered R. The flow diagram displayed in Figure 1 is used in the model development, and Table 1 has a complete list of all model parameters. The fractal-fractional operator in the Atangana-Baleanu sense, which is a useful tool for studying epidemic dynamics and disease transmission, as well as for simulating complex systems and phenomena, has been introduced in this article. This approach can be used to real-world problems since it can depict fractal processes as well as fractional-order dynamics.

According to the Atangana-Baleanu sense, the new fractional model for $0 < \varpi, \vartheta \leq 1$ is made up of the following non-linear fractal-fractional differential equations.

$$ \begin{aligned}
{}_{0}^{FFM}D_t^{\varpi,\vartheta}S(t) &= \mu^{\varpi}N^{\varpi} + \Phi^{\varpi}V_1 - \frac{\beta^{\varpi}S(I+C)}{N^{\varpi}} - \Lambda^{\varpi}S \\
&\quad - \mu^{\varpi}S, \\
{}_{0}^{FFM}D_t^{\varpi,\vartheta}V_1(t) &= \Lambda^{\varpi}S - \Phi^{\varpi}V_1 - \eta^{\varpi}V_1 - \mu^{\varpi}V_1, \\
{}_{0}^{FFM}D_t^{\varpi,\vartheta}V_2(t) &= \eta^{\varpi}V_1 - \chi^{\varpi}V_2 - (1-\xi^{\varpi})r_1^{\varpi}V_2 - \mu^{\varpi}V_2, \\
{}_{0}^{FFM}D_t^{\varpi,\vartheta}V_3(t) &= \chi^{\varpi}V_2 - r_1^{\varpi}V_3 - \mu^{\varpi}V_3, \\
{}_{0}^{FFM}D_t^{\varpi,\vartheta}E(t) &= \frac{\beta^{\varpi}S(I+C)}{N^{\varpi}} - \delta^{\varpi}E - \mu^{\varpi}E, \\
{}_{0}^{FFM}D_t^{\varpi,\vartheta}I(t) &= \alpha^{\varpi}\delta^{\varpi}E - h_1^{\varpi}I - r_2^{\varpi}I - \mu^{\varpi}I, \\
{}_{0}^{FFM}D_t^{\varpi,\vartheta}C(t) &= (1-\alpha^{\varpi})\delta^{\varpi}E - h_2^{\varpi}C - r_3^{\varpi}C - \mu^{\varpi}C, \\
{}_{0}^{FFM}D_t^{\varpi,\vartheta}H(t) &= h_1^{\varpi}I + h_2^{\varpi}C - r_4^{\varpi}H - \mu^{\varpi}H, \\
{}_{0}^{FFM}D_t^{\varpi,\vartheta}R(t) &= (1-\xi^{\varpi})r_1^{\varpi}V_2 + r_1^{\varpi}V_3 + r_2^{\varpi}I + r_3^{\varpi}C \\
&\quad + r_4^{\varpi}H - \mu^{\varpi}R,
\end{aligned} \tag{7} $$

with the initial conditions is given as

$$ \begin{aligned}
&S(0) \geq 0, \quad V_1(0) \geq 0, \quad V_2(0) \geq 0, \\
&V_3(0) \geq 0, \quad E(0) \geq 0, \quad I(0) \geq 0, \\
&C(0) \geq 0, \quad H(0) \geq 0, \quad R(0) \geq 0.
\end{aligned} $$

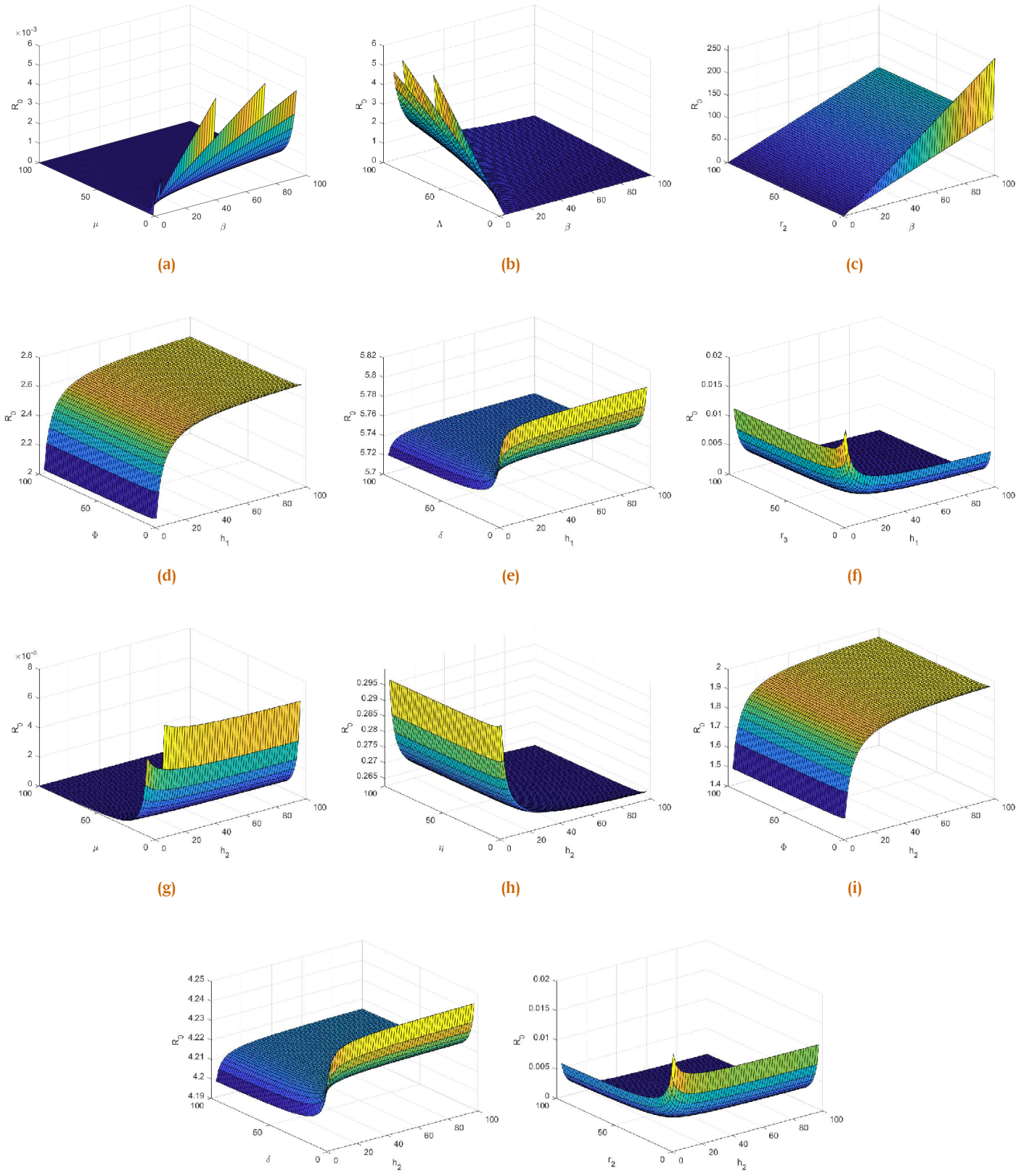

Figure 2. Effect of parameters on reproductive number

3.1. Positively invariant region

Lemma 1. *The region* $\Im_l \in \mathbb{R}_+^9$

$$\Im_l = \left\{(S, V_1, V_2, V_3, E, I, C, H, R) \in \mathbb{R}_+^9 : 0 \leq N\right\}$$

generates all solutions for the system (7), and under non-negative initial conditions, is positively invariant for the system shown in $\mathbb{R}_+^9$.

Proof. Using system (7), we discover that

$$\begin{aligned}
{}_0^{FFM}D_t^{\varpi,\vartheta} S(t)|_{S=0} &= \mu^{\varpi} N^{\varpi} + \Phi^{\varpi} V_1 \geq 0,\\
{}_0^{FFM}D_t^{\varpi,\vartheta} V_1(t)|_{V_1=0} &= \Lambda^{\varpi} S \geq 0,\\
{}_0^{FFM}D_t^{\varpi,\vartheta} V_2(t)|_{V_2=0} &= \eta^{\varpi} V_1 \geq 0,\\
{}_0^{FFM}D_t^{\varpi,\vartheta} V_3(t)|_{V_3=0} &= \chi^{\varpi} V_2 \geq 0,\\
{}_0^{FFM}D_t^{\varpi,\vartheta} E(t)|_{E=0} &= \frac{\beta^{\varpi} S(I+C)}{N^{\varpi}} \geq 0,\\
{}_0^{FFM}D_t^{\varpi,\vartheta} I(t)|_{I=0} &= \alpha^{\varpi}\delta^{\varpi} E \geq 0,\\
{}_0^{FFM}D_t^{\varpi,\vartheta} C(t)|_{C=0} &= (1-\alpha^{\varpi})\delta^{\varpi} E \geq 0,\\
{}_0^{FFM}D_t^{\varpi,\vartheta} H(t)|_{H=0} &= h_1^{\varpi} I + h_2^{\varpi} C \geq 0,\\
{}_0^{FFM}D_t^{\varpi,\vartheta} R(t)|_{R=0} &= (1-\xi^{\varpi}) r_1^{\varpi} V_2 + r_1^{\varpi} V_3 + r_2^{\varpi} I\\
&\quad + r_3^{\varpi} C + r_4^{\varpi} H \geq 0.
\end{aligned} \tag{8}$$

As a result, S,V_1, V_2, V_3,E,I,C, and R are nonnegative. They are therefore also bounded. □

3.2. Equilibrium point and reproductive number

This section covers equilibrium points in detail. We solve the system to obtain equilibrium points system (7).

$$\begin{aligned}
E_{\bullet} &= (S^{\bullet}, V_1^{\bullet}, V_2^{\bullet}, V_3^{\bullet}, E^{\bullet}, I^{\bullet}, C^{\bullet}, H^{\bullet}, R^{\bullet})\\
&= \left(\frac{c_1\mu^{\varpi}N^{\varpi}}{c_7}, \frac{\Lambda^{\varpi}\mu^{\varpi}N^{\varpi}}{c_7}, \frac{\mu^{\varpi}\eta^{\varpi}\Lambda^{\varpi}N^{\varpi}}{c_4c_7},\right.\\
&\quad \left.\frac{\mu^{\varpi}\eta^{\varpi}\chi^{\varpi}\Lambda^{\varpi}N^{\varpi}}{c_4c_3c_7}, 0, 0, 0, 0, \frac{\eta^{\varpi}r_1^{\varpi}a_{10}\Lambda^{\varpi}N^{\varpi}}{c_4c_7}\right),
\end{aligned} \tag{9}$$

where

$$\begin{aligned}
&c_1 = \Phi^{\varpi} + \eta^{\varpi} + \mu^{\varpi},\ c_2 = \Lambda^{\varpi} + \mu^{\varpi},\ c_3 = r_1^{\varpi} + \mu^{\varpi},\\
&c_5 = h_1^{\varpi} + r_2^{\varpi} + \mu^{\varpi},\ c_6 = \delta^{\varpi} + \mu^{\varpi},\ c_8 = h_2^{\varpi} + r_3^{\varpi} + \mu^{\varpi},\\
&c_4 = \chi^{\varpi} + \mu^{\varpi} + (1-\xi^{\varpi}) r_1^{\varpi},\ c_{10} = r_4^{\varpi} + \mu^{\varpi}\\
&c_7 = (\Lambda^{\varpi} + \mu^{\varpi})(\Phi^{\varpi} + \eta^{\varpi} + \mu^{\varpi}) - \Lambda^{\varpi}\Phi^{\varpi},\\
&c_9 = (1-\xi^{\varpi}) + \frac{\chi^{\varpi}}{r_1^{\varpi} + \mu^{\varpi}}.
\end{aligned}$$

The fundamental reproductive number is provided as

$$R_0 = \frac{(\alpha^{\varpi} c_8 + (1-\alpha^{\varpi}) c_5)\beta^{\varpi}\delta^{\varpi}\mu^{\varpi} c_1}{c_5 c_6 c_7 c_8} \tag{10}$$

The analysis of the impact of individual R_0 components is presented in Figure 2.

The endemic equilibrium, is then presented as

$$\begin{aligned}
E_{\otimes} &= \left(S^{\otimes}, V_1^{\otimes}, V_2^{\otimes}, V_3^{\otimes}, E^{\otimes}, I^{\otimes}, C^{\otimes}, H^{\otimes}, R^{\otimes}\right),\\
S^{\otimes} &= \frac{c_1\mu^{\varpi}N^{\varpi}}{c_7R_0},\ V_1^{\otimes} = \frac{\mu^{\varpi}\Lambda^{\varpi}N^{\varpi}}{c_7R_0},\ V_2^{\otimes} = \frac{\mu^{\varpi}\eta\Lambda^{\varpi}N^{\varpi}}{c_4c_7R_0},\\
E^{\otimes} &= \frac{c_5c_7c_8N^{\varpi}(R_0-1)}{\beta^{\varpi}\delta^{\varpi}c_1(c_8\alpha^{\varpi} + c_5(1-\alpha^{\varpi}))},\ V_3^{\otimes} = \frac{\chi^{\varpi}\mu^{\varpi}\eta^{\varpi}\Lambda^{\varpi}N^{\varpi}}{c_3c_4c_7R_0},\\
I^{\otimes} &= \frac{c_7c_8\alpha^{\varpi}N^{\varpi}(R_0-1)}{\beta^{\varpi}c_1(c_8\alpha^{\varpi} + c_5(1-\alpha^{\varpi}))},\\
C^{\otimes} &= \frac{(1-\alpha^{\varpi})c_5c_7N^{\varpi}(R_0-1)}{\beta^{\varpi}c_1(c_8\alpha^{\varpi} + c_5(1-\alpha^{\varpi}))},\\
H^{\otimes} &= \frac{c_7N^{\varpi}(R_0-1)}{\beta^{\varpi}\delta^{\varpi}c_1c_7(c_8\alpha^{\varpi} + c_5(1-\alpha^{\varpi}))}\left(h_1^{\varpi}c_8\alpha^{\varpi} + h_2^{\varpi}c_5(1\right.\\
&\quad \left.-\alpha^{\varpi})\right),\\
R^{\otimes} &= \frac{c_9r_1^{\varpi}\eta^{\varpi}\Lambda^{\varpi}N^{\varpi}}{c_4c_7} + \frac{c_2c_7N^{\varpi}(R_0-1)}{\beta^{\varpi}\delta^{\varpi}c_1(c_8\alpha^{\varpi} + c_5(1-\alpha^{\varpi}))}.
\end{aligned} \tag{11}$$

The presence of the endemic equilibrium $E_{\otimes}$ is determined by the value of R_0. The following variables are positive if $R_0 > 1$, $S^{\otimes}, V_1^{\otimes}, V_2^{\otimes}, V_3^{\otimes}, E^{\otimes}, I^{\otimes}, C^{\otimes}, H^{\otimes}, R^{\otimes}$. The system (8) has a unique endemic equilibrium for $R_0 > 1$, and no positive endemic equilibrium when $R_0 < 1$.

3.3. Sensitivity analysis

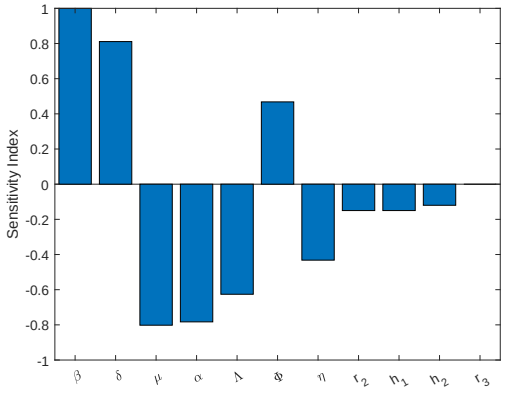

Figure 3. Sensitivity Indices of R_0 with respect to various parameters

The sensitivity analysis objective is to identify the factors that influence the COVID-19 virus ability to spread. R_0 sensitivity index depends on how well its component parts are differentiated. The reproduction number will rise in value if the parameter value increases, according to the positive sign of the sensitivity index, whereas the reproduction number will fall in value if the parameter value increases. Sensitivity Indices of R_0 with respect to various parameters are show in Figure 3.

$$\begin{aligned}
\frac{\partial R_0}{\partial\beta^{\varpi}} &= \frac{\delta^{\varpi}\mu^{\varpi}(\alpha^{\varpi}c_8 - (\alpha^{\varpi}-1)c_5)c_1}{c_5c_6c_7c_8} \times \frac{\beta^{\varpi}}{R_0} > 0,\\
\frac{\partial R_0}{\partial\delta^{\varpi}} &= \frac{\beta^{\varpi}\mu^{\varpi}(\alpha^{\varpi}c_8 - (\alpha^{\varpi}-1)c_5)c_1}{c_5c_6c_7c_8}\\
&\quad - \frac{\beta^{\varpi}\delta^{\varpi}\mu^{\varpi}(\alpha^{\varpi}c_8 - (\alpha^{\varpi}-1)c_5)c_1}{(\delta^{\varpi}+\mu^{\varpi})^2c_5c_7c_8} \times \frac{\delta^{\varpi}}{R_0} > 0,
\end{aligned}$$

$$\frac{\partial R_0}{\partial \mu^{\varpi}} = \frac{\beta^{\varpi}\delta^{\varpi}\mu^{\varpi}c_1}{c_2c_5c_6c_7c_8} + \frac{\beta^{\varpi}\delta^{\varpi}\mu^{\varpi}\left(\alpha^{\varpi}c_8-(\alpha^{\varpi}-1)c_5\right)}{c_5c_6c_7c_8} + \frac{\beta^{\varpi}\delta^{\varpi}\left(\alpha^{\varpi}c_8-(\alpha^{\varpi}-1)c_5\right)c_1}{c_5c_6c_7c_8} - \frac{\beta^{\varpi}\delta^{\varpi}\mu^{\varpi}\left(\alpha^{\varpi}c_8-(\alpha^{\varpi}-1)c_5\right)c_1}{c_5c_6c_7c_8^2} - \frac{\beta^{\varpi}\delta^{\varpi}\mu^{\varpi}\left(\alpha^{\varpi}c_8-(\alpha^{\varpi}-1)c_5\right)c_1}{c_5^2c_6c_7c_8} - \frac{\beta^{\varpi}\delta^{\varpi}\mu^{\varpi}\left(\alpha^{\varpi}c_8-(\alpha^{\varpi}-1)c_5\right)c_1}{c_5c_6^2c_7c_8} - \frac{\beta^{\varpi}\delta^{\varpi}\mu^{\varpi}\left(\alpha^{\varpi}c_8-(\alpha^{\varpi}-1)c_5\right)c_1c_7}{c_5c_6c_7^2c_8}\times\frac{\mu^{\varpi}}{R_0}<0,$$

$$\frac{\partial R_0}{\partial \alpha^{\varpi}} = -\frac{\beta^{\varpi}\delta^{\varpi}\mu^{\varpi}c_1\left(c_5-c_8\right)}{c_5c_6c_7c_8}\times\frac{\alpha^{\varpi}}{R_0}<0,$$

$$\frac{\partial R_0}{\partial \Lambda^{\varpi}} = -\frac{\beta^{\varpi}\delta^{\varpi}\mu^{\varpi}\left(\eta^{\varpi}+\mu^{\varpi}\right)\left(\alpha^{\varpi}c_8-(\alpha^{\varpi}-1)c_5\right)c_1}{c_5c_6c_7^2c_8}\times\frac{\Lambda^{\varpi}}{R_0}<0,$$

$$\frac{\partial R_0}{\partial \Phi^{\varpi}} = \frac{\beta^{\varpi}\delta^{\varpi}\mu^{\varpi}\left(\alpha^{\varpi}c_8-(\alpha^{\varpi}-1)c_5\right)}{c_5c_6c_7c_8} - \frac{\beta^{\varpi}\delta^{\varpi}\mu^{\varpi 2}\left(\alpha^{\varpi}c_8-(\alpha^{\varpi}-1)c_5\right)c_1}{c_5c_6c_7^2c_8}\times\frac{\Phi^{\varpi}}{R_0}>0,$$

$$\frac{\partial R_0}{\partial \eta^{\varpi}} = -\frac{\beta^{\varpi}\delta^{\varpi}\mu^{\varpi}\left(\Lambda^{\varpi}+\mu^{\varpi}\right)\left(\alpha^{\varpi}c_8-(\alpha^{\varpi}-1)c_5\right)c_1}{c_5c_6c_7^2c_8}\times\frac{\eta^{\varpi}}{R_0} + \frac{\beta^{\varpi}\delta^{\varpi}\mu^{\varpi}\left(\alpha^{\varpi}c_8-(\alpha^{\varpi}-1)c_5\right)}{c_5c_6c_7c_8}<0,$$

$$\frac{\partial R_0}{\partial r_2^{\varpi}} = -\frac{\beta^{\varpi}\delta^{\varpi}\mu^{\varpi}\left(\alpha^{\varpi}-1\right)c_1}{c_5c_6c_7c_8} - \frac{\beta^{\varpi}\delta^{\varpi}\mu^{\varpi}\left(\alpha^{\varpi}c_8-(\alpha^{\varpi}-1)c_5\right)c_1}{c_5^2c_6c_7c_8}\times\frac{r_2^{\varpi}}{R_0}<0,$$

$$\frac{\partial R_0}{\partial h_1^{\varpi}} = -\frac{\beta^{\varpi}\delta^{\varpi}\mu^{\varpi}\left(\alpha^{\varpi}-1\right)c_1}{c_5c_6c_7c_8} - \frac{\beta^{\varpi}\delta^{\varpi}\mu^{\varpi}\left(\alpha^{\varpi}c_8-(\alpha^{\varpi}-1)c_5\right)c_1}{c_5^2c_6c_7c_8}\times\frac{h_1^{\varpi}}{R_0}<0,$$

$$\frac{\partial R_0}{\partial h_2^{\varpi}} = \frac{\alpha^{\varpi}\beta^{\varpi}\delta^{\varpi}\mu^{\varpi}c_1}{c_5c_6c_7c_8} - \frac{\beta^{\varpi}\delta^{\varpi}\mu^{\varpi}\left(\alpha^{\varpi}c_8-(\alpha^{\varpi}-1)c_5\right)c_1}{c_5c_6c_7c_8^2}\times\frac{h_2^{\varpi}}{R_0}<0,$$

$$\frac{\partial R_0}{\partial r_3^{\varpi}} = \frac{\alpha^{\varpi}\beta^{\varpi}\delta^{\varpi}\mu^{\varpi}c_1}{c_5c_6c_7c_8} - \frac{\beta^{\varpi}\delta^{\varpi}\mu^{\varpi}\left(\alpha^{\varpi}c_8-(\alpha^{\varpi}-1)c_5\right)c_1}{c_5c_6c_7c_8^2}\times\frac{r_3^{\varpi}}{R_0}<0.$$

4. Existence and Uniqueness Result

We get the existence and uniqueness of the model using the fractal fractional Atangana-Baleanu technique. Consider

$$\begin{aligned}
{}_0^{FFM}D_t^{\varpi,\vartheta}S(t) &= \mu^{\varpi}N^{\varpi}+\Phi^{\varpi}V_1-\frac{\beta^{\varpi}S(I+C)}{N^{\varpi}}-\Lambda^{\varpi}S-\mu^{\varpi}S,\\
{}_0^{FFM}D_t^{\varpi,\vartheta}V_1(t) &= \Lambda^{\varpi}S-\Phi^{\varpi}V_1-\eta^{\varpi}V_1-\mu^{\varpi}V_1,\\
{}_0^{FFM}D_t^{\varpi,\vartheta}V_2(t) &= \eta^{\varpi}V_1-\chi^{\varpi}V_2-(1-\xi^{\varpi})r_1^{\varpi}V_2-\mu^{\varpi}V_2,\\
{}_0^{FFM}D_t^{\varpi,\vartheta}V_3(t) &= \chi^{\varpi}V_2-r_1^{\varpi}V_3-\mu^{\varpi}V_3,\\
{}_0^{FFM}D_t^{\varpi,\vartheta}E(t) &= \frac{\beta^{\varpi}S(I+C)}{N^{\varpi}}-\delta^{\varpi}E-\mu^{\varpi}E,\\
{}_0^{FFM}D_t^{\varpi,\vartheta}I(t) &= \alpha^{\varpi}\delta^{\varpi}E-h_1^{\varpi}I-r_2^{\varpi}I-\mu^{\varpi}I,\\
{}_0^{FFM}D_t^{\varpi,\vartheta}C(t) &= (1-\alpha^{\varpi})\delta^{\varpi}E-h_2^{\varpi}C-r_3^{\varpi}C-\mu^{\varpi}C,\\
{}_0^{FFM}D_t^{\varpi,\vartheta}H(t) &= h_1^{\varpi}I+h_2^{\varpi}C-r_4^{\varpi}H-\mu^{\varpi}H,\\
{}_0^{FFM}D_t^{\varpi,\vartheta}R(t) &= (1-\xi^{\varpi})r_1^{\varpi}V_2+r_1^{\varpi}V_3+r_2^{\varpi}I+r_3^{\varpi}C+r_4^{\varpi}H-\mu^{\varpi}R.
\end{aligned} \tag{12}$$

We demonstrate that the considered model has a unique solution at least once through the use of fixed point results. Since integral meets the differentiability criterion, we can represent the model as

$$\begin{aligned}
S(t) &= S(0)+\frac{\vartheta(1-\varpi)t^{\vartheta-1}}{\mathcal{AB}(\varpi)}\tilde{S}(t,S(t)) + \frac{\varpi\vartheta}{\mathcal{AB}(\varpi)\Gamma(\varpi)}\int_0^t(t-\varsigma)^{\varpi-1}\varsigma^{\vartheta-1}\tilde{S}(\varsigma,S(\varsigma))d\varsigma\\
&= \mathcal{A}_1+\mathcal{A}_2,\\
V_1(t) &= V_1(0)+\frac{\vartheta(1-\varpi)t^{\vartheta-1}}{\mathcal{AB}(\varpi)}\tilde{V}_1(t,V_1(t)) + \frac{\varpi\vartheta}{\mathcal{AB}(\varpi)\Gamma(\varpi)}\int_0^t(t-\varsigma)^{\varpi-1}\varsigma^{\vartheta-1}\tilde{V}_1(\varsigma,V_1(\varsigma))d\varsigma\\
&= \mathcal{B}_1+\mathcal{B}_2,\\
V_2(t) &= V_2(0)+\frac{\vartheta(1-\varpi)t^{\vartheta-1}}{\mathcal{AB}(\varpi)}\tilde{V}_2(t,V_2(t)) + \frac{\varpi\vartheta}{\mathcal{AB}(\varpi)\Gamma(\varpi)}\int_0^t(t-\varsigma)^{\varpi-1}\varsigma^{\vartheta-1}\tilde{V}_2(\varsigma,V_2(\varsigma))d\varsigma\\
&= \mathcal{C}_1+\mathcal{C}_2,\\
V_3(t) &= V_3(0)+\frac{\vartheta(1-\varpi)t^{\vartheta-1}}{\mathcal{AB}(\varpi)}\tilde{V}_3(t,V_3(t)) + \frac{\varpi\vartheta}{\mathcal{AB}(\varpi)\Gamma(\varpi)}\int_0^t(t-\varsigma)^{\varpi-1}\varsigma^{\vartheta-1}\tilde{V}_3(\varsigma,V_3(\varsigma))d\varsigma\\
&= \mathcal{D}_1+\mathcal{D}_2,\\
E(t) &= E(0)+\frac{\vartheta(1-\varpi)t^{\vartheta-1}}{\mathcal{AB}(\varpi)}\tilde{E}(t,E(t)) + \frac{\varpi\vartheta}{\mathcal{AB}(\varpi)\Gamma(\varpi)}\int_0^t(t-\varsigma)^{\varpi-1}\varsigma^{\vartheta-1}\tilde{E}(\varsigma,E(\varsigma))d\varsigma\\
&= \mathcal{E}_1+\mathcal{E}_2,\\
I(t) &= I(0)+\frac{\vartheta(1-\varpi)t^{\vartheta-1}}{\mathcal{AB}(\varpi)}\tilde{I}(t,I(t)) + \frac{\varpi\vartheta}{\mathcal{AB}(\varpi)\Gamma(\varpi)}\int_0^t(t-\varsigma)^{\varpi-1}\varsigma^{\vartheta-1}\tilde{I}(\varsigma,I(\varsigma))d\varsigma\\
&= \mathcal{F}_1+\mathcal{F}_2,\\
C(t) &= C(0)+\frac{\vartheta(1-\varpi)t^{\vartheta-1}}{\mathcal{AB}(\varpi)}\tilde{C}(t,C(t)) + \frac{\varpi\vartheta}{\mathcal{AB}(\varpi)\Gamma(\varpi)}\int_0^t(t-\varsigma)^{\varpi-1}\varsigma^{\vartheta-1}\tilde{C}(\varsigma,C(\varsigma))d\varsigma\\
&= \mathcal{G}_1+\mathcal{G}_2,
\end{aligned} \tag{13}$$

$$
\begin{aligned}
H(t) &= H(0) + \frac{\vartheta(1-\varpi)t^{\vartheta-1}}{\mathcal{AB}(\varpi)}\tilde{H}(t,H(t)) \\
&\quad + \frac{\varpi\vartheta}{\mathcal{AB}(\varpi)\Gamma(\varpi)}\int_0^t (t-\varsigma)^{\varpi-1}\varsigma^{\vartheta-1}\tilde{H}(\varsigma,H(\varsigma))d\varsigma \\
&= \mathcal{H}_1 + \mathcal{H}_2, \\
R(t) &= R(0) + \frac{\vartheta(1-\varpi)t^{\vartheta-1}}{\mathcal{AB}(\varpi)}\tilde{R}(t,R(t)) \\
&\quad + \frac{\varpi\vartheta}{\mathcal{AB}(\varpi)\Gamma(\varpi)}\int_0^t (t-\varsigma)^{\varpi-1}\varsigma^{\vartheta-1}\tilde{R}(\varsigma,R(\varsigma))d\varsigma \\
&= \mathcal{I}_1 + \mathcal{I}_2.
\end{aligned}
$$

$$
\begin{aligned}
\mathcal{A}_1 &= S(0) + \frac{\vartheta(1-\varpi)t^{\vartheta-1}}{\mathcal{AB}(\varpi)}\tilde{S}(t,S(t)), \\
\mathcal{B}_1 &= V_1(0) + \frac{\vartheta(1-\varpi)t^{\vartheta-1}}{\mathcal{AB}(\varpi)}\tilde{V}_2(t,V_2(t)), \\
\mathcal{C}_1 &= V_2(0) + \frac{\vartheta(1-\varpi)t^{\vartheta-1}}{\mathfrak{AB}(\varpi)}\tilde{V}_2(t,V_2(t)), \\
\mathcal{D}_1 &= V_3(0) + \frac{\vartheta(1-\varpi)t^{\vartheta-1}}{\mathcal{AB}(\varpi)}\tilde{V}_3(t,V_3(t)), \\
\mathcal{E}_1 &= E(0) + \frac{\vartheta(1-\varpi)t^{\vartheta-1}}{\mathfrak{AB}(\varpi)}\tilde{E}(t,E(t)), \\
\mathcal{F}_1 &= I(0) + \frac{\vartheta(1-\varpi)t^{\vartheta-1}}{\mathcal{AB}(\varpi)}\tilde{I}(t,I(t)), \\
\mathcal{G}_1 &= C(0) + \frac{\vartheta(1-\varpi)t^{\vartheta-1}}{\mathfrak{AB}(\varpi)}\tilde{C}(t,C(t)), \\
\mathcal{H}_1 &= H(0) + \frac{\vartheta(1-\varpi)t^{\vartheta-1}}{\mathcal{AB}(\varpi)}\tilde{H}(t,H(t)), \\
\mathcal{I}_1 &= R(0) + \frac{\vartheta(1-\varpi)t^{\vartheta-1}}{\mathfrak{AB}(\varpi)}\tilde{R}(t,R(t)).
\end{aligned} \tag{14}
$$

$$
\begin{aligned}
\mathcal{A}_2 &= \frac{\varpi\vartheta}{\mathcal{AB}(\varpi)\Gamma(\varpi)}\int_0^t (t-\varsigma)^{\varpi-1}\varsigma^{\vartheta-1}\tilde{S}(\varsigma,S(\varsigma))d\varsigma, \\
\mathcal{B}_\in &= \frac{\varpi\vartheta}{\mathcal{AB}(\varpi)\Gamma(\varpi)}\int_0^t (t-\varsigma)^{\varpi-1}\varsigma^{\vartheta-1}\tilde{V}_1(\varsigma,V_1(\varsigma))d\varsigma, \\
\mathcal{C}_2 &= \frac{\varpi\vartheta}{\mathcal{AB}(\varpi)\Gamma(\varpi)}\int_0^t (t-\varsigma)^{\varpi-1}\varsigma^{\vartheta-1}\tilde{V}_2(\varsigma,V_2(\varsigma))d\varsigma, \\
\mathcal{D}_2 &= \frac{\varpi\vartheta}{\mathcal{AB}(\varpi)\Gamma(\varpi)}\int_0^t (t-\varsigma)^{\varpi-1}\varsigma^{\vartheta-1}\tilde{V}_3(\varsigma,V_3(\varsigma))d\varsigma, \\
\mathcal{E}_2 &= \frac{\varpi\vartheta}{\mathcal{AB}(\varpi)\Gamma(\varpi)}\int_0^t (t-\varsigma)^{\varpi-1}\varsigma^{\vartheta-1}\tilde{E}(\varsigma,E(\varsigma))d\varsigma, \\
\mathcal{F}_2 &= \frac{\varpi\vartheta}{\mathcal{AB}(\varpi)\Gamma(\varpi)}\int_0^t (t-\varsigma)^{\varpi-1}\varsigma^{\vartheta-1}\tilde{I}(\varsigma,I(\varsigma))d\varsigma, \\
\mathcal{G}_2 &= \frac{\varpi\vartheta}{\mathcal{AB}(\varpi)\Gamma(\varpi)}\int_0^t (t-\varsigma)^{\varpi-1}\varsigma^{\vartheta-1}\tilde{C}(\varsigma,C(\varsigma))d\varsigma, \\
\mathcal{H}_2 &= \frac{\varpi\vartheta}{\mathcal{AB}(\varpi)\Gamma(\varpi)}\int_0^t (t-\varsigma)^{\varpi-1}\varsigma^{\vartheta-1}\tilde{H}(\varsigma,H(\varsigma))d\varsigma, \\
\mathcal{I}_2 &= \frac{\varpi\vartheta}{\mathcal{AB}(\varpi)\Gamma(\varpi)}\int_0^t (t-\varsigma)^{\varpi-1}\varsigma^{\vartheta-1}\tilde{R}(\varsigma,R(\varsigma))d\varsigma.
\end{aligned} \tag{15}
$$

We present the essential feature of the governing formulas eq. (13), the function $\clubsuit(\mathcal{A}_1,\mathcal{B}_1,\mathcal{C}_1,\mathcal{D}_1,\mathcal{E}_1,\mathcal{F}_1,\mathcal{G}_1,\mathcal{H}_1,\mathcal{I}_1)$ as contraction mappings, and the function $\spadesuit(\mathcal{A}_2,\mathcal{B}_2,\mathcal{C}_2,\mathcal{D}_2,\mathcal{E}_2,\mathcal{F}_2,\mathcal{G}_2,\mathcal{H}_2,\mathcal{I}_2)$ as continuous and compact integral components, by means of Krasnoselski's fixed point theorem.

Theorem 1. *The non-linear mapping*

$$\clubsuit(\mathcal{A}_1,\mathcal{B}_1,\mathcal{C}_1,\mathcal{D}_1,\mathcal{E}_1,\mathcal{F}_1,\mathcal{G}_1,\mathcal{H}_1,\mathcal{I}_1):[0,\mathbb{T}]\times\mathbb{R}\to\mathbb{R}^9$$

described in eqs. (14) and (15) guarantees that positive constants $¶_1, ¶_2, ¶_3, ¶_4, ¶_5, ¶_6, ¶_7, ¶_8, ¶_9$ *satisfy the Lipschitz contractive condition.*

Proof. Examine the operator $\clubsuit(\mathcal{A}_1,\mathcal{B}_1,\mathcal{C}_1,\mathcal{D}_1,\mathcal{E}_1,\mathcal{F}_1,\mathcal{G}_1,\mathcal{H}_1,\mathcal{I}_1):[0,\mathbb{T}]\times\mathbb{R}\to\mathbf{R}^9$ in a structure of an entire normed space.

$$
\begin{aligned}
\|(S,V_1,V_2,V_3,E,I,C,H,R)\| = \max_{t\in[0,\mathbb{T}]} \big\| & S(t)+V_1(t)+V_2(t) \\
& + V_3(t)+E(t)+I(t)+C(t) \\
& + H(t)+R(t)\big\|
\end{aligned} \tag{16}
$$

with $S,V_1,V_2,V_3,E,I,C,H,R\in[0,\mathbb{T}]$.

Starting with, we will observe that $\clubsuit(\mathcal{A}_1,\mathcal{B}_1,\mathcal{C}_1,\mathcal{D}_1,\mathcal{E}_1,\mathcal{F}_1,\mathcal{G}_1,\mathcal{H}_1,\mathcal{I}_1)$ serves as a mapping of contractions. The behavior for S and $\tilde{S}$ will be discovered.

$$
\begin{aligned}
\|\Psi_1-\Psi_2\| &= \left\| \left(\mu^\varpi N^\varpi + \Phi^\varpi V_1 - \Lambda^\varpi S - \frac{\beta^\varpi S\,(I+C)}{N^\varpi} - \mu^\varpi S\right) - \left(\mu^\varpi N^\varpi + \Phi^\varpi V_1 - \frac{\beta^\varpi \tilde{S}\,(I+C)}{N^\varpi} - \Lambda^\varpi\tilde{S} - \mu^\varpi\tilde{S}\right)\right\|, \\
&\le \left\| \left(\frac{\beta^\varpi\,(I+C)}{N^\varpi} + \Lambda^\varpi + \mu^\varpi\right)\left(S-\tilde{S}\right)\right\|, \\
&\le \left\| \left(\frac{\beta^\varpi\,(\|I\|+\|C\|)}{N^\varpi} + \Lambda^\varpi + \mu^\varpi\right)\right\| \left\|\left(S-\tilde{S}\right)\right\|, \\
&\le ¶_1\left\|\left(S-\tilde{S}\right)\right\|, \\
\Psi_1 &= \zeta_1\,(S,V_1,V_2,V_3,E,I,C,H,R)\,(t)\,, \\
\Psi_2 &= \zeta_1\left(\tilde{S},V_1,V_2,V_3,E,I,C,H,R\right)(t)\,, \\
¶_1 &= \left\| \left(\frac{\beta^\varpi\,(\|I\|+\|C\|)}{N^\varpi} + \Lambda^\varpi + \mu^\varpi\right)\right|.
\end{aligned} \tag{17}
$$

With this method, we are able to

$$
\begin{aligned}
¶_2\|(V_1-\tilde{V_1})\| &\ge \big\|\zeta_2(S,V_1,V_2,V_3,E,I,C,H,R)(t) - \zeta_2(S,\tilde{V_1},V_2,V_3,E,I,C,H,R)(t)\big\| \\
¶_3\|(V_2-\tilde{V_2})\| &\ge \big\|\zeta_3(S,V_1,V_2,V_3,E,I,C,H,R)(t) - \zeta_3(S,V_1,\tilde{V_2},V_3,E,I,C,H,R)(t)\big\|, \\
¶_4\|(V_3-\tilde{V_3})\| &\ge \big\|\zeta_4(S,V_1,V_2,V_3,E,I,C,H,R)(t) - \zeta_4(S,V_1,V_2,\tilde{V_3},E,I,C,H,R)(t)\big\|, \\
¶_5\|(E-\tilde{E})\| &\ge \big\|\zeta_5(S,V_1,V_2,V_3,E,I,C,H,R)(t) - \zeta_5(S,V_1,V_2,V_3,\tilde{E},I,C,H,R)(t)\big\|, \\
¶_6\|(I-\tilde{I})\| &\ge \big\|\zeta_6(S,V_1,V_2,V_3,E,I,C,H,R)(t) - \zeta_6(S,V_1,V_2,V_3,E,\tilde{I},C,H,R)(t)\big\|,
\end{aligned}
$$

$$
\begin{aligned}
\P_7\|(C-\tilde{C})\| &\geq \big\|\zeta_7(S,V_1,V_2,V_3,E,I,C,H,R)(t)\\
&\quad-\zeta_7(S,V_1,V_2,V_3,E,I,\tilde{C},H,R)(t)\big\|,\\
\P_8\|(H-\tilde{H})\| &\geq \big\|\zeta_8(S,V_1,V_2,V_3,E,I,C,H,R)(t)\\
&\quad-\zeta_8(S,V_1,V_2,V_3,E,I,C,\tilde{H},R)(t)\big\|,\\
\P_9\|(R-\tilde{R})\| &\geq \big\|\zeta_9(S,V_1,V_2,V_3,E,I,C,H,R)(t)\\
&\quad-\zeta_9(S,V_1,V_2,V_3,E,I,C,H,\tilde{R})(t)\big\|,\\
\P_2 &= \|\eta^{\varpi}+\mu^{\varpi}\|, \quad \P_4 = \|r_1^{\varpi}+\mu^{\varpi}\|,\\
\P_3 &= \|\chi^{\varpi}+(1+\xi^{\varpi})\,r_1^{\varpi}+\mu^{\varpi}\|,\\
\P_5 &= \|\delta^{\varpi}+\mu^{\varpi}\|, \quad \P_8 = \|r_4^{\varpi}+\mu^{\varpi}\|,\\
\P_6 &= \|h_1^{\varpi}+r_2^{\varpi}+\mu^{\varpi}\|, \quad \P_9 = \|\mu^{\varpi}\|,\\
\P_7 &= \|h_2^{\varpi}+r_3^{\varpi}-\mu^{\varpi}\|
\end{aligned}
\tag{18}
$$

Consequently, we could derive the following for $\clubsuit(S,V_1,V_2,V_3,E,I,C,H)$:

$$
\begin{aligned}
\|\Psi_3-\Psi_4\| &= \frac{\vartheta(1-\varpi)t^{\vartheta-1}}{\mathcal{AB}(\varpi)}\max_{t\in[0,\mathbb{T}]}\big|(S,V_1,V_2,V_3,E,I,C,H,R)(t)\\
&\quad-(\tilde{S},\tilde{V}_1,\tilde{V}_2,\tilde{V}_3,\tilde{E},\tilde{I},\tilde{C},\tilde{H},\tilde{R})(t)\big|\\
&\leq \frac{\vartheta(1-\varpi)t^{\vartheta-1}}{\mathcal{AB}(\varpi)}\big\|(S,V_1,V_2,V_3,E,I,C,H,R)(t)\\
&\quad-(\tilde{S},\tilde{V}_1,\tilde{V}_2,\tilde{V}_3,\tilde{E},\tilde{I},\tilde{C},\tilde{H},\tilde{R})(t)\big\|\\
&\leq \frac{\vartheta(1-\varpi)t^{\vartheta-1}}{\mathcal{AB}(\varpi)}\P,\\
\Psi_3 &= \clubsuit(S,V_1,V_2,V_3,E,I,C,H,R)(t),\\
\Psi_4 &= \clubsuit(\tilde{S},\tilde{V}_1,\tilde{V}_2,\tilde{V}_3,\tilde{E},\tilde{I},\tilde{C},\tilde{H},\tilde{R})(t).
\end{aligned}
$$

The following gives the Lipschitz constant: $\P=\max[\P_1,\P_2,\P_3,\P_4,\P_5,\P_6,\P_7,\P_8,\P_9]<1$. This suggests that $\clubsuit(\zeta_1,\zeta_2,\zeta_3,\zeta_4,\zeta_5,\zeta_6,\zeta_7,\zeta_8,\zeta_9)$ is a non-expansive operator. Next, we'll demonstrate that $\spadesuit(\mathcal{A}_2,\mathcal{B}_2,\mathcal{C}_2,\mathcal{D}_2,\mathcal{E}_2,\mathcal{F}_2,\mathcal{G}_2,\mathcal{H}_2,\mathcal{I}_2)$ is compact and continuous. The constrained operators' absolute norms $\zeta_1,\zeta_2,\zeta_3,\zeta_4,\zeta_5,\zeta_6,\zeta_7,\zeta_8$ and ζ_9 given in eqs. (14) and (15) are non-zero positive constants $\wp_1,\wp_2,\wp_3,\wp_4,\wp_5,\wp_6,\wp_7,\wp_8,\wp_9,\beth_1,\beth_2,\beth_3,\beth_4,\beth_5,\beth_6,\beth_7,\beth_8,\beth_9$. These constants fulfill the following boundedness inequalities, proving the operator's compactness $\spadesuit(\mathcal{A}_2,\mathcal{B}_2,\mathcal{C}_2,\mathcal{D}_2,\mathcal{E}_2,\mathcal{F}_2,\mathcal{G}_2,\mathcal{H}_2,\mathcal{I}_2)$.

$$
\begin{array}{llll}
|\zeta_1(t,S)| \leq \wp_1\|S\|+\beth_1, & |\zeta_2(t,V_1)| \leq \wp_2\|V_1\|+\beth_2,\\
|\zeta_3(t,V_2)| \leq \wp_3\|V_2\|+\beth_3, & |\zeta_4(t,V_3)| \leq \wp_4\|V_3\|+\beth_4,\\
|\zeta_5(t,E)| \leq \wp_5\|E\|+\beth_5, & |\zeta_6(t,I)| \leq \wp_6\|I\|+\beth_6,\\
|\zeta_7(t,C)| \leq \wp_7\|C\|+\beth_7, & |\zeta_8(t,H)| \leq \wp_8\|H\|+\beth_8,\\
|\zeta_9(t,R)| \leq \wp_9\|R\|+\beth_9. &
\end{array}
\tag{19}
$$

Assume that $\mathcal{P}$ is a closed subset of $\mathcal{Z}$.

$$
\begin{aligned}
\mathcal{P}=\big\{&(\zeta_1,\zeta_2,\zeta_3,\zeta_4,\zeta_5,\zeta_6,\zeta_7,\zeta_8,\zeta_9)\in\mathcal{Z}\|\zeta_1,\zeta_2,\zeta_3,\zeta_4,\zeta_5,\\
&\zeta_6,\zeta_7,\zeta_8,\zeta_9\|\leq\Omega,\ \Omega>0\big\}
\end{aligned}
$$

$(\zeta_1,\zeta_2,\zeta_3,\zeta_4,\zeta_5,\zeta_6,\zeta_7,\zeta_8,\zeta_9)\in\mathcal{P}$, we find

$$
\begin{aligned}
\|\mathcal{A}_2(t,S)\| &= \max_{t\in[0,\mathbb{T}]}\Big|\frac{\varpi\vartheta}{\mathcal{AB}(\varpi)\Gamma(\varpi)}\int_0^t(t-\varsigma)^{\varpi-1}\varsigma^{\vartheta-1}\zeta_1(\varsigma,S(\varsigma))d\varsigma\Big|\\
&\leq \frac{\urcorner^{\varpi,\vartheta}}{\mathcal{AB}(\varpi)\Gamma(\varpi)}\int_0^{\urcorner}(\urcorner-\varsigma)^{\varpi-1}\varsigma^{\vartheta-1}\big|\mathcal{A}(\varsigma,S(\varsigma))\big|d\varsigma\\
&\leq \frac{\urcorner^{\varpi,\vartheta}}{\mathcal{AB}(\varpi)\Gamma(\varpi)}\eta_1\omega+\varsigma_1.
\end{aligned}
\tag{20}
$$

This has been verified for further components in a similar way. Next, identify the maximum norm possible. $\|\beth(\mathcal{A}_2,\mathcal{B}_2,\mathcal{C}_2,\mathcal{D}_2,\mathcal{E}_2,\mathcal{F}_2,\mathcal{G}_2,\mathcal{H}_2,\mathcal{I}_2)\|$ as follows:

$$
\begin{aligned}
\|\beth(\mathcal{A}_2,\mathcal{B}_2,\mathcal{C}_2,\mathcal{D}_2,\mathcal{E}_2,\mathcal{F}_2,\mathcal{G}_2,\mathcal{H}_2,\mathcal{I}_2))\| &\leq \Big\{\big[\wp_1+\wp_2+\wp_3+\wp_4+\wp_5\\
&\quad+\wp_6+\wp_7+\wp_8+\wp_9\big]\Omega+\beth_1\\
&\quad+\beth_2+\beth_3+\beth_4+\beth_5+\beth_6+\beth_7\\
&\quad+\beth_8+\beth_9\Big\}\\
&= \Upsilon,
\end{aligned}
\tag{21}
$$

where a positive constant is indicated by Υ. Hence, $|\beth(S,V_1,V_2,V_3,E,I,C,H,R)|\leq\Upsilon)$, it suggests that the operator $\beth$ is uniformly bounded.

We shall now demonstrate that the continuous function $\beth$ is uniform for $t_x<t_y\in[0,\mathbb{T}]$. To accomplish this, consider $t_1<t_2\in[0,\mathbb{T}]$.

$$
\begin{aligned}
|\mathcal{A}_2(t_2,S)-\mathcal{A}_2(t_1,S)| &= \Big|\int_0^{t_y}(t-\varsigma)^{\varpi-1}\varsigma^{\vartheta-1}\zeta_1(\varsigma,S(\varsigma))d\varsigma\\
&\quad-\int_0^{t_x}(t-\varsigma)^{\varpi-1}\varsigma^{\vartheta-1}\zeta_1[\varsigma,S(\varsigma)]d\varsigma\Big|\\
&\quad\times\frac{\varpi\vartheta}{\mathcal{AB}(\varpi)\Gamma(\varpi)}\\
&\leq \frac{\varpi\vartheta}{\mathcal{AB}(\varpi)\Gamma(\varpi)}\Big[\int_0^{t_y}(t-\varsigma)^{\varpi-1}\varsigma^{\vartheta-1}\\
&\quad-\int_0^{t_x}(t-\varsigma)^{\varpi-1}\varsigma^{\vartheta-1}\Big]\big(\wp_1\Omega+\beth_1\big)\\
&\leq \frac{\wp_1\vartheta+\varsigma_1}{\mathcal{AB}(\varpi)\Gamma(\varpi)}\Big[t_2^{\varpi,\vartheta}-t_1^{\varpi,\vartheta}\Big].
\end{aligned}
\tag{22}
$$

Similarly,

$$
\begin{aligned}
\big|\mathcal{B}_2(t_2,V_1)-\mathcal{B}_2(t_1,V_1)\big| &\leq \frac{\wp_2\Omega+\beth_2}{\mathcal{AB}(\varpi)\Gamma(\varpi)}\big(t_2^{\varpi,\vartheta}-t_1^{\varpi,\vartheta}\big),\\
\big|\mathcal{C}_2(t_2,V_2)-\mathcal{C}_2(t_1,V_2)\big| &\leq \frac{\wp_3\Omega+\beth_3}{\mathcal{AB}(\varpi)\Gamma(\varpi)}\big(t_2^{\varpi,\vartheta}-t_1^{\varpi,\vartheta}\big),\\
\big|\mathcal{D}_2(t_2,V_3)-\mathcal{D}_2(t_1,V_3)\big| &\leq \frac{\wp_4\Omega+\beth_4}{\mathcal{AB}(\varpi)\Gamma(\varpi)}\big(t_2^{\varpi,\vartheta}-t_1^{\varpi,\vartheta}\big),\\
\big|\mathcal{E}_2(t_2,E)-\mathcal{E}_2(t_1,E)\big| &\leq \frac{\wp_5\Omega+\beth_5}{\mathcal{AB}(\varpi)\Gamma(\varpi)}\big(t_2^{\varpi,\vartheta}-t_1^{\varpi,\vartheta}\big),\\
\big|\mathcal{F}_2(t_2,I)-\mathcal{F}_2(t_1,I)\big| &\leq \frac{\wp_6\Omega+\beth_6}{\mathcal{AB}(\varpi)\Gamma(\varpi)}\big(t_2^{\varpi,\vartheta}-t_1^{\varpi,\vartheta}\big),\\
\big|\mathcal{G}_2(t_2,C)-\mathcal{G}_2(t_1,C)\big| &\leq \frac{\wp_7\Omega+\beth_7}{\mathcal{AB}(\varpi)\Gamma(\varpi)}\big(t_2^{\varpi,\vartheta}-t_1^{\varpi,\vartheta}\big),
\end{aligned}
$$

$$\left|\mathcal{H}_2(t_2,H)-\mathcal{H}_2(t_1,H)\right| \le \frac{\wp_8\Omega+\beth_8}{\mathcal{AB}(\varpi)\Gamma(\varpi)}\left(t_2^{\varpi,\vartheta}-t_1^{\varpi,\vartheta}\right),$$
$$\left|\mathcal{I}_2(t_2,R)-\mathcal{I}_2(t_1,R)\right| \le \frac{\wp_9\Omega+\beth_9}{\mathcal{AB}(\varpi)\Gamma(\varpi)}\left(t_2^{\varpi,\vartheta}-t_1^{\varpi,\vartheta}\right). \quad (23)$$

As $t_2 \to t_1$, the result is independent of $(S, V_1, V_2, V_3, E, I, C, H, R)$. This implies that

$$\begin{matrix}\left\|\beth(\mathcal{A}_2,\mathcal{B}_2,\mathcal{C}_2,\mathcal{D}_2,\mathcal{E}_2,\mathcal{F}_2,\mathcal{G}_2,\mathcal{H}_2,\mathcal{I}_2)(t_2)\right. & \to & 0\\ \left.-\beth(\mathcal{A}_2,\mathcal{B}_2,\mathcal{C}_2,\mathcal{D}_2,\mathcal{E}_2,\mathcal{F}_2,\mathcal{G}_2,\mathcal{H}_2,\mathcal{I}_2)(t_1)\right\| & & \end{matrix} \quad (24)$$

$\beth(\mathcal{A}_2, \mathcal{B}_2, \mathcal{C}_2, \mathcal{D}_2, \mathcal{E}_2, \mathcal{F}_2, \mathcal{G}_2, \mathcal{H}_2, \mathcal{I}_2)$ is therefore compact and equicontinuous, as well as completely continuous, by the Arzela theorem.
The Krasnoselskii theorem thus indicates that the existence of a unique singular solution is guaranteed by the compactness of the operators ♣ and ♠. □

Theorem 2. *The solution of system (7) is unique if*

$$\frac{\urcorner^{\varpi,\vartheta}}{\mathcal{AB}(\varpi)\Gamma(\varpi)}\psi \le 1 \quad (25)$$

$\urcorner = \max\{\urcorner_1, \urcorner_2, \urcorner_3, \urcorner_4, \urcorner_5, \urcorner_6, \urcorner_7, \urcorner_8, \urcorner_9\}$

Proof. Consider an operator $\rho = (\rho_1, \rho_2, \rho_3, \rho_4, \rho_5, \rho_6, \rho_7, \rho_8, \rho_9) : \mathcal{Z} \to \mathcal{Z}$ applying eq. (19) in this way:

$$\rho_1(S)(t) = S(0) + \frac{\vartheta(1-\varpi)t^{\vartheta-1}}{\mathcal{AB}(\varpi)}\zeta_1(t,S(t)) + \frac{\varpi\vartheta}{\mathcal{AB}(\varpi)\Gamma(\varpi)}\int_0^t (t-\varsigma)^{\varpi-1}\varsigma^{\vartheta-1}\zeta_1(\varsigma,S(\varsigma))d\varsigma,$$
$$\rho_2(V_1)(t) = V_1(0) + \frac{\vartheta(1-\varpi)t^{\vartheta-1}}{\mathcal{AB}(\varpi)}\zeta_2(t,V_1(t)) + \frac{\varpi\vartheta}{\mathcal{AB}(\varpi)\Gamma(\varpi)}\int_0^t (t-\varsigma)^{\varpi-1}\varsigma^{\vartheta-1}\zeta_2(\varsigma,V_1(\varsigma))d\varsigma,$$
$$\rho_3(V_2)(t) = V_2(0) + \frac{\vartheta(1-\varpi)t^{\vartheta-1}}{\mathcal{AB}(\varpi)}\zeta_3(t,V_2(t)) + \frac{\varpi\vartheta}{\mathcal{AB}(\varpi)\Gamma(\varpi)}\int_0^t (t-\varsigma)^{\varpi-1}\varsigma^{\vartheta-1}\zeta_3(\varsigma,V_2(\varsigma))d\varsigma,$$
$$\rho_4(V_3)(t) = V_3(0) + \frac{\vartheta(1-\varpi)t^{\vartheta-1}}{\mathcal{AB}(\varpi)}\zeta_4(t,V_3(t)) + \frac{\varpi\vartheta}{\mathcal{AB}(\varpi)\Gamma(\varpi)}\int_0^t (t-\varsigma)^{\varpi-1}\varsigma^{\vartheta-1}\zeta_4(\varsigma,V_3(\varsigma))d\varsigma,$$
$$\rho_5(E)(t) = E(0) + \frac{\vartheta(1-\varpi)t^{\vartheta-1}}{\mathcal{AB}(\varpi)}\zeta_5(t,E(t)) + \frac{\varpi\vartheta}{\mathcal{AB}(\varpi)\Gamma(\varpi)}\int_0^t (t-\varsigma)^{\varpi-1}\varsigma^{\vartheta-1}\zeta_5(\varsigma,E(\varsigma))d\varsigma,$$
$$\rho_6(I)(t) = I(0) + \frac{\vartheta(1-\varpi)t^{\vartheta-1}}{\mathcal{AB}(\varpi)}\zeta_6(t,I(t)) + \frac{\varpi\vartheta}{\mathcal{AB}(\varpi)\Gamma(\varpi)}\int_0^t (t-\varsigma)^{\varpi-1}\varsigma^{\vartheta-1}\zeta_6(\varsigma,I(\varsigma))d\varsigma,$$
$$\rho_7(C)(t) = C(0) + \frac{\vartheta(1-\varpi)t^{\vartheta-1}}{\mathcal{AB}(\varpi)}\zeta_7(t,C(t)) + \frac{\varpi\vartheta}{\mathcal{AB}(\varpi)\Gamma(\varpi)}\int_0^t (t-\varsigma)^{\varpi-1}\varsigma^{\vartheta-1}\zeta_7(\varsigma,C(\varsigma))d\varsigma,$$
$$\rho_8(H)(t) = H(0) + \frac{\vartheta(1-\varpi)t^{\vartheta-1}}{\mathcal{AB}(\varpi)}\zeta_8(t,H(t)) + \frac{\varpi\vartheta}{\mathcal{AB}(\varpi)\Gamma(\varpi)}\int_0^t (t-\varsigma)^{\varpi-1}\varsigma^{\vartheta-1}\zeta_8(\varsigma,H(\varsigma))d\varsigma,$$
$$\rho_9(R)(t) = R(0) + \frac{\vartheta(1-\varpi)t^{\vartheta-1}}{\mathcal{AB}(\varpi)}\zeta_9(t,R(t)) + \frac{\varpi\vartheta}{\mathcal{AB}(\varpi)\Gamma(\varpi)}\int_0^t (t-\varsigma)^{\varpi-1}\varsigma^{\vartheta-1}\zeta_9(\varsigma,C(\varsigma))d\varsigma. \quad (26)$$

For $(S,V_1,V_2,V_3,E,I,C,H,R)$, $(\tilde{S},\tilde{V}_1,\tilde{V}_2,\tilde{V}_3,\tilde{E},\tilde{I},\tilde{C},\tilde{H},\tilde{R}) \in \mathcal{Z}$, and utilizing eq. (22) we get,

$$\begin{aligned}\left\|\rho_1(S)(t)-\rho_1(\tilde{S})(t)\right\| &= \frac{\vartheta(1-\varpi)t^{\vartheta-1}}{\mathcal{AB}(\varpi)}\left\|\zeta_1(t,S(t))-\zeta_1(t,\tilde{S}(t))\right\| + \frac{\varpi\vartheta}{\mathcal{AB}(\varpi)\Gamma(\varpi)}\int_0^t \|\zeta_1(\varsigma,S(\varsigma)) - \zeta_1(\varsigma,\tilde{S}(\varsigma))\|(t-\varsigma)^{\varpi-1}\varsigma^{\vartheta-1}\zeta_1(\varsigma,S(\varsigma))d\varsigma \\ &\le \frac{\vartheta(1-\varpi)t^{\vartheta-1}}{\mathcal{AB}(\varpi)}\urcorner_1\|S-\tilde{S}\| \end{aligned} \quad (27)$$

$$\begin{aligned}&+ \frac{\varsigma^{\varpi,\vartheta}}{\mathcal{AB}(\varpi)\Gamma(\varpi)}\urcorner_1\|S-\tilde{S}\| \\ &\le \urcorner_1\|S-\tilde{S}\|\left[\frac{\vartheta(1-\varpi)t^{\vartheta-1}}{\mathcal{AB}(\varpi)} + \frac{\varsigma^{\varpi,\vartheta}}{\mathcal{AB}(\varpi)\Gamma(\varpi)}\right] \end{aligned} \quad (28)$$

$\|S-\tilde{S}\| \to 0$ when $S \to \tilde{S}$. Hence

$$\left\|\rho_1(S)(t)-\rho_1(\tilde{S})(t)\right\| \le \left[\frac{\vartheta(1-\varpi)t^{\vartheta-1}}{\mathcal{AB}(\varpi)} + \frac{\varsigma^{\varpi,\vartheta}}{\mathcal{AB}(\varpi)\Gamma(\varpi)}\right]\urcorner_1 \le 1 \quad (29)$$

with

$$\left\|\rho_1(S)(t)-\rho_1(\tilde{S})(t)\right\|\left[1-\left(\frac{\vartheta(1-\varpi)t^{\vartheta-1}}{\mathcal{AB}(\varpi)} + \frac{\varsigma^{\varpi,\vartheta}}{\mathcal{AB}(\varpi)\Gamma(\varpi)}\right)\urcorner_1\right] \le 0 \quad (30)$$

With this approach, we discover

$$\begin{aligned}\left\|\Psi_5-\Psi_6\right\| \le \left(\frac{\vartheta(1-\varpi)t^{\vartheta-1}}{\mathcal{AB}(\varpi)} + \frac{\varsigma^{\varpi,\vartheta}}{\mathcal{AB}(\varpi)\Gamma(\varpi)}\right)\urcorner\|(S,V_1,V_2,V_3,\\ E,I,C,H,R)-(\tilde{S},\tilde{V}_1,\tilde{V}_2,\tilde{V}_3,\tilde{E},\tilde{I},\tilde{C},\tilde{H},\tilde{R})\|,\\ \Psi_5 = \rho(S,V_1,V_2,V_3,E,I,C,H,R)(t),\\ \Psi_6 = \rho(\tilde{S},\tilde{V}_1,\tilde{V}_2,\tilde{V}_3,\tilde{E},\tilde{I},\tilde{C},\tilde{H},\tilde{R})(t).\end{aligned} \quad (31)$$

We ensure that our proposed model has a unique fixed-point solution by including the properties of both the Schauder and Krasnoselskii theorems into the contraction mapping Υ. □

5. Ulam-Hyers Stability

$$\wp_1 \ge \left|S(t) + \left(\frac{\vartheta(1-\varpi)t^{\vartheta-1}}{\mathcal{AB}(\varpi)}\right)\Xi_1(t,S(t))\right.$$

$$+\left(\frac{\varpi\vartheta}{\mathcal{AB}(\varpi)}\int_0^t(t-\varsigma)\varsigma^{\varpi-1}\right)\Xi_1(t,S(t))\,d\varsigma\Big|,$$

$$\wp_2\geq\Big|V_1(t)+\left(\frac{\vartheta(1-\varpi)t^{\vartheta-1}}{\mathcal{AB}(\varpi)}\right)\Xi_2(t,V_1(t))$$
$$+\left(\frac{\varpi\vartheta}{\mathcal{AB}(\varpi)}\int_0^t(t-\varsigma)\varsigma^{\varpi-1}\right)\Xi_2(t,V_1(t))\,d\varsigma\Big|,$$

$$\wp_3\geq\Big|V_2(t)+\left(\frac{\vartheta(1-\varpi)t^{\vartheta-1}}{\mathcal{AB}(\varpi)}\right)\Xi_3(t,V_2(t))$$
$$+\left(\frac{\varpi\vartheta}{\mathcal{AB}(\varpi)}\int_0^t(t-\varsigma)\varsigma^{\varpi-1}\right)\Xi_3(t,V_2(t))\,d\varsigma\Big|,$$

$$\wp_4\geq\Big|V_3(t)+\left(\frac{\vartheta(1-\varpi)t^{\vartheta-1}}{\mathcal{AB}(\varpi)}\right)\Xi_4(t,V_3(t))$$
$$+\left(\frac{\varpi\vartheta}{\mathcal{AB}(\varpi)}\int_0^t(t-\varsigma)\varsigma^{\varpi-1}\right)\Xi_4(t,V_3(t))\,d\varsigma\Big|,$$

$$\wp_5\geq\Big|E(t)+\left(\frac{\vartheta(1-\varpi)t^{\vartheta-1}}{\mathcal{AB}(\varpi)}\right)\Xi_5(t,E(t))$$
$$+\left(\frac{\varpi\vartheta}{\mathcal{AB}(\varpi)}\int_0^t(t-\varsigma)\varsigma^{\varpi-1}\right)\Xi_5(t,E(t))\,d\varsigma\Big|,$$

$$\wp_6\geq\Big|I(t)+\left(\frac{\vartheta(1-\varpi)t^{\vartheta-1}}{\mathcal{AB}(\varpi)}\right)\Xi_6(t,I(t))$$
$$+\left(\frac{\varpi\vartheta}{\mathcal{AB}(\varpi)}\int_0^t(t-\varsigma)\varsigma^{\varpi-1}\right)\Xi_6(t,I(t))\,d\varsigma\Big|,$$

$$\wp_7\geq\Big|C(t)+\left(\frac{\vartheta(1-\varpi)t^{\vartheta-1}}{\mathcal{AB}(\varpi)}\right)\Xi_7(t,C(t))$$
$$+\left(\frac{\varpi\vartheta}{\mathcal{AB}(\varpi)}\int_0^t(t-\varsigma)\varsigma^{\varpi-1}\right)\Xi_7(t,C(t))\,d\varsigma\Big|,$$

$$\wp_8\geq\Big|H(t)+\left(\frac{\vartheta(1-\varpi)t^{\vartheta-1}}{\mathcal{AB}(\varpi)}\right)\Xi_8(t,H(t))$$
$$+\left(\frac{\varpi\vartheta}{\mathcal{AB}(\varpi)}\int_0^t(t-\varsigma)\varsigma^{\varpi-1}\right)\Xi_8(t,H(t))\,d\varsigma\Big|,$$

$$\wp_9\geq\Big|R(t)+\left(\frac{\vartheta(1-\varpi)t^{\vartheta-1}}{\mathcal{AB}(\varpi)}\right)\Xi_9(t,R(t))$$
$$+\left(\frac{\varpi\vartheta}{\mathcal{AB}(\varpi)}\int_0^t(t-\varsigma)\varsigma^{\varpi-1}\right)\Xi_9(t,R(t))\,d\varsigma\Big|,\quad(32)$$

there exist $\tilde{S},\tilde{V}_1,\tilde{V}_2,\tilde{V}_3,\tilde{E},\tilde{I},\tilde{C},\tilde{H}$ and $\tilde{R}$.

$$\tilde{S}(t)=\left(\frac{\vartheta(1-\varpi)t^{\vartheta-1}}{\mathcal{AB}(\varpi)}\right)\Xi_1\left(t,\tilde{S}(t)\right)$$
$$+\left(\frac{\varpi\vartheta}{\mathcal{AB}(\varpi)}\int_0^t(t-\varsigma)\varsigma^{\varpi-1}\right)\Xi_1\left(t,\tilde{S}(t)\right)d\varsigma,$$

$$\tilde{V}_1(t)=\left(\frac{\vartheta(1-\varpi)t^{\vartheta-1}}{\mathcal{AB}(\varpi)}\right)\Xi_2\left(t,\tilde{V}_1(t)\right)$$
$$+\left(\frac{\varpi\vartheta}{\mathcal{AB}(\varpi)}\int_0^t(t-\varsigma)\varsigma^{\varpi-1}\right)\Xi_2\left(t,\tilde{V}_1(t)\right)d\varsigma,$$

$$\tilde{V}_2(t)=\left(\frac{\vartheta(1-\varpi)t^{\vartheta-1}}{\mathcal{AB}(\varpi)}\right)\Xi_3\left(t,\tilde{V}_2(t)\right)$$
$$+\left(\frac{\varpi\vartheta}{\mathcal{AB}(\varpi)}\int_0^t(t-\varsigma)\varsigma^{\varpi-1}\right)\Xi_3\left(t,\tilde{V}_2(t)\right)d\varsigma,$$

$$\tilde{V}_3(t)=\left(\frac{\vartheta(1-\varpi)t^{\vartheta-1}}{\mathcal{AB}(\varpi)}\right)\Xi_4\left(t,\tilde{V}_3(t)\right)$$
$$+\left(\frac{\varpi\vartheta}{\mathcal{AB}(\varpi)}\int_0^t(t-\varsigma)\varsigma^{\varpi-1}\right)\Xi_4\left(t,\tilde{V}_3(t)\right)d\varsigma,$$

$$\tilde{E}(t)=\left(\frac{\vartheta(1-\varpi)t^{\vartheta-1}}{\mathcal{AB}(\varpi)}\right)\Xi_5\left(t,\tilde{E}(t)\right)$$
$$+\left(\frac{\varpi\vartheta}{\mathcal{AB}(\varpi)}\int_0^t(t-\varsigma)\varsigma^{\varpi-1}\right)\Xi_5\left(t,\tilde{E}(t)\right)d\varsigma,$$

$$\tilde{I}(t)=\left(\frac{\vartheta(1-\varpi)t^{\vartheta-1}}{\mathcal{AB}(\varpi)}\right)\Xi_6\left(t,\tilde{I}(t)\right)$$
$$+\left(\frac{\varpi\vartheta}{\mathcal{AB}(\varpi)}\int_0^t(t-\varsigma)\varsigma^{\varpi-1}\right)\Xi_6\left(t,\tilde{I}(t)\right)d\varsigma,$$

$$\tilde{C}(t)=\left(\frac{\vartheta(1-\varpi)t^{\vartheta-1}}{\mathcal{AB}(\varpi)}\right)\Xi_7\left(t,\tilde{C}(t)\right)$$
$$+\left(\frac{\varpi\vartheta}{\mathcal{AB}(\varpi)}\int_0^t(t-\varsigma)\varsigma^{\varpi-1}\right)\Xi_7\left(t,\tilde{C}(t)\right)d\varsigma,$$

$$\tilde{H}(t)=\left(\frac{\vartheta(1-\varpi)t^{\vartheta-1}}{\mathcal{AB}(\varpi)}\right)\Xi_8\left(t,\tilde{H}(t)\right)$$
$$+\left(\frac{\varpi\vartheta}{\mathcal{AB}(\varpi)}\int_0^t(t-\varsigma)\varsigma^{\varpi-1}\right)\Xi_8\left(t,\tilde{H}(t)\right)d\varsigma,$$

$$\tilde{R}(t)=\left(\frac{\vartheta(1-\varpi)t^{\vartheta-1}}{\mathcal{AB}(\varpi)}\right)\Xi_9\left(t,\tilde{R}(t)\right)$$
$$+\left(\frac{\varpi\vartheta}{\mathcal{AB}(\varpi)}\int_0^t(t-\varsigma)\varsigma^{\varpi-1}\right)\Xi_9\left(t,\tilde{R}(t)\right)d\varsigma,\quad(33)$$

such that

$$label34\quad\begin{array}{llll}\|S(t)-\tilde{S}\| & \leq & \wp_1\Psi_1, & \|V_1(t)-\tilde{V}_1\| \leq \wp_2\Psi_2,\\ \|V_2(t)-\tilde{V}_2\| & \leq & \wp_3\Psi_3, & \|V_3(t)-\tilde{V}_3\| \leq \wp_4\Psi_4,\\ \|E(t)-\tilde{E}\| & \leq & \wp_5\Psi_5, & \|I(t)-\tilde{I}\| \leq \wp_6\Psi_6,\\ \|C(t)-\tilde{C}\| & \leq & \wp_7\Psi_7, & \|H(t)-\tilde{H}\| \leq \wp_8\Psi_8,\\ \|R(t)-\tilde{R}\| & \leq & \wp_9\Psi_9. & \end{array}\quad(34)$$

Theorem 3. *Let $S(t)$, $V_1(t)$, $V_2(t)$, $V_3(t)$, $E(t)$, $I(t)$, $C(t)$, $H(t)$, $R(t)$ and $\tilde{S}(t)$, $\tilde{V}_1(t)$, $\tilde{V}_2(t)$, $\tilde{V}_3(t)$, $\tilde{E}(t)$, $\tilde{I}(t)$, $\tilde{C}(t)$, $\tilde{H}(t)$, $\tilde{R}(t)$ are constant functions that ensure that*

$$\begin{array}{cccccccc} \|S(t)\| & \leq & \Phi_1, & \|V_1(t)\| & \leq & \Phi_2, & \|V_2(t)\| & \leq & \Phi_3, \\ \|V_3(t)\| & \leq & \Phi_4, & \|E(t)\| & \leq & \Phi_5, & \|I(t)\| & \leq & \Phi_6, \\ \|C(t)\| & \leq & \Phi_7, & \|H(t)\| & \leq & \Phi_8, & \|R(t)\| & \leq & \Phi_9. \end{array} \tag{35}$$

If this condition is satisfied, Ulam-Hyers stability for the fractional system (7) exists.

Proof. A solution has been found for $S(t)$, $V_1(t)$, $V_2(t)$, $V_3(t)$, $E(t)$, $I(t)$, $C(t)$, $H(t)$, $R(t)$. Assume that $\tilde{S}(t)$, $\tilde{V}_1(t)$, $\tilde{V}_2(t)$, $\tilde{V}_3(t)$, $\tilde{E}(t)$, $\tilde{I}(t)$, $\tilde{C}(t)$, $\tilde{H}(t)$, $\tilde{R}(t)$ are our system's approximations, and they satisfy the following requirements.

$$\begin{aligned} \left\|S(t)-\tilde{S}(t)\right\| &\leq \frac{\vartheta(1-\varpi)t^{\vartheta-1}}{\mathcal{AB}(\varpi)}\Phi_1\left(t,\tilde{S}(t)\right) \\ &\quad+\frac{\varpi\vartheta}{\mathcal{AB}(\varpi)}\int_0^t(t-\varsigma)^{\varpi-1}\Phi_1\left(t,\tilde{S}(t)\right)d\varsigma \\ &\leq \frac{\vartheta(1-\varpi)t^{\vartheta-1}+\varpi\vartheta}{\mathcal{AB}(\varpi)}\Phi_1\left\|S(t)-\tilde{S}(t)\right\|. \end{aligned} \tag{36}$$

Consider $\Phi_i=\wp_i$ and $\Psi_i=\frac{\vartheta(1-\varpi)t^{\vartheta-1}+\varpi\vartheta}{\mathcal{AB}(\varpi)}$ for $i=1,2,3,\ldots,9$, we have

$$\left\|S(t)-\tilde{S}(t)\right\|\leq\wp_1\Psi_1 \tag{37}$$

similarly,

$$\begin{aligned} \left\|V_1(t)-\tilde{V}_1(t)\right\| &\leq \frac{\vartheta(1-\varpi)t^{\vartheta-1}}{\mathcal{AB}(\varpi)}\Phi_2\left(t,\tilde{V}_1(t)\right) \\ &\quad+\frac{\varpi\vartheta}{\mathcal{AB}(\varpi)}\int_0^t(t-\varsigma)^{\varpi-1}\Phi_2\left(t,\tilde{V}_1(t)\right)d\varsigma \\ &\leq \frac{\vartheta(1-\varpi)t^{\vartheta-1}+\varpi\vartheta}{\mathcal{AB}(\varpi)}\Phi_2\left\|V_1(t)-\tilde{V}_1(t)\right\|, \end{aligned} \tag{38}$$

$$\begin{aligned} \left\|V_2(t)-\tilde{V}_2(t)\right\| &\leq \frac{\vartheta(1-\varpi)t^{\vartheta-1}}{\mathcal{AB}(\varpi)}\Phi_3\left(t,\tilde{V}_2(t)\right) \\ &\quad+\frac{\varpi\vartheta}{\mathcal{AB}(\varpi)}\int_0^t(t-\varsigma)^{\varpi-1}\Phi_3\left(t,\tilde{V}_2(t)\right)d\varsigma \\ &\leq \frac{\vartheta(1-\varpi)t^{\vartheta-1}+\varpi\vartheta}{\mathcal{AB}(\varpi)}\Phi_3\left\|V_2(t)-\tilde{V}_2(t)\right\|, \end{aligned} \tag{39}$$

$$\begin{aligned} \left\|V_3(t)-\tilde{V}_3(t)\right\| &\leq \frac{\vartheta(1-\varpi)t^{\vartheta-1}}{\mathcal{AB}(\varpi)}\Phi_4\left(t,\tilde{V}_3(t)\right) \\ &\quad+\frac{\varpi\vartheta}{\mathcal{AB}(\varpi)}\int_0^t(t-\varsigma)^{\varpi-1}\Phi_4\left(t,\tilde{V}_3(t)\right)d\varsigma \\ &\leq \frac{\vartheta(1-\varpi)t^{\vartheta-1}+\varpi\vartheta}{\mathcal{AB}(\varpi)}\Phi_4\left\|V_3(t)-\tilde{V}_3(t)\right\|, \end{aligned} \tag{40}$$

$$\begin{aligned} \left\|E(t)-\tilde{E}(t)\right\| &\leq \frac{\vartheta(1-\varpi)t^{\vartheta-1}}{\mathcal{AB}(\varpi)}\Phi_5\left(t,\tilde{E}(t)\right) \\ &\quad+\frac{\varpi\vartheta}{\mathcal{AB}(\varpi)}\int_0^t(t-\varsigma)^{\varpi-1}\Phi_5\left(t,\tilde{E}(t)\right)d\varsigma \\ &\leq \frac{\vartheta(1-\varpi)t^{\vartheta-1}+\varpi\vartheta}{\mathcal{AB}(\varpi)}\Phi_5\left\|E(t)-\tilde{E}(t)\right\|, \end{aligned} \tag{41}$$

$$\begin{aligned} \left\|I(t)-\tilde{I}(t)\right\| &\leq \frac{\vartheta(1-\varpi)t^{\vartheta-1}}{\mathcal{AB}(\varpi)}\Phi_6\left(t,\tilde{I}(t)\right) \\ &\quad+\frac{\varpi\vartheta}{\mathcal{AB}(\varpi)}\int_0^t(t-\varsigma)^{\varpi-1}\Phi_6\left(t,\tilde{I}(t)\right)d\varsigma \\ &\leq \frac{\vartheta(1-\varpi)t^{\vartheta-1}+\varpi\vartheta}{\mathcal{AB}(\varpi)}\Phi_6\left\|I(t)-\tilde{I}(t)\right\|,, \end{aligned} \tag{42}$$

$$\begin{aligned} \left\|C(t)-\tilde{C}(t)\right\| &\leq \frac{\vartheta(1-\varpi)t^{\vartheta-1}}{\mathcal{AB}(\varpi)}\Phi_7\left(t,\tilde{C}(t)\right) \\ &\quad+\frac{\varpi\vartheta}{\mathcal{AB}(\varpi)}\int_0^t(t-\varsigma)^{\varpi-1}\Phi_7\left(t,\tilde{C}(t)\right)d\varsigma \\ &\leq \frac{\vartheta(1-\varpi)t^{\vartheta-1}+\varpi\vartheta}{\mathcal{AB}(\varpi)}\Phi_7\left\|C(t)-\tilde{C}(t)\right\|, \end{aligned} \tag{43}$$

$$\begin{aligned} \left\|H(t)-\tilde{H}(t)\right\| &\leq \frac{\vartheta(1-\varpi)t^{\vartheta-1}}{\mathcal{AB}(\varpi)}\Phi_8\left(t,\tilde{H}(t)\right) \\ &\quad+\frac{\varpi\vartheta}{\mathcal{AB}(\varpi)}\int_0^t(t-\varsigma)^{\varpi-1}\Phi_8\left(t,\tilde{H}(t)\right)d\varsigma \\ &\leq \frac{\vartheta(1-\varpi)t^{\vartheta-1}+\varpi\vartheta}{\mathcal{AB}(\varpi)}\Phi_8\left\|H(t)-\tilde{H}(t)\right\|, \end{aligned} \tag{44}$$

$$\begin{aligned} \left\|R(t)-\tilde{R}(t)\right\| &\leq \frac{\vartheta(1-\varpi)t^{\vartheta-1}}{\mathcal{AB}(\varpi)}\Phi_9\left(t,\tilde{R}(t)\right) \\ &\quad+\frac{\varpi\vartheta}{\mathcal{AB}(\varpi)}\int_0^t(t-\varsigma)^{\varpi-1}\Phi_9\left(t,\tilde{R}(t)\right)d\varsigma \\ &\leq \frac{\vartheta(1-\varpi)t^{\vartheta-1}+\varpi\vartheta}{\mathcal{AB}(\varpi)}\Phi_9\left\|R(t)-\tilde{R}(t)\right\|. \end{aligned} \tag{45}$$

These differences indicate the Ulam-Hyers stability of the system. □

6. PID and Controllability

It was examined in [4] using the COVID-19 model. Given below is the COVID mathematical model:

$$\dot{S}(t)=\mu N+\Phi V_1-\frac{\beta S(I+C)}{N}-\Lambda S-\mu S,$$

$$\begin{aligned}
\dot{V}_1(t) &= \Lambda S - \Phi V_1 - \eta V_1 - \mu V_1,\\
\dot{V}_2(t) &= \eta V_1 - \chi V_2 - (1-\xi) r_1 V_2 - \mu V_2,\\
\dot{V}_3(t) &= \chi V_2 - r_1 V_3 - \mu V_3,\\
\dot{E}(t) &= \frac{\beta S(I+C)}{N} - \delta E - \mu E,\\
\dot{I}(t) &= \alpha\delta E - h_1 I - r_2 I - \mu I,\\
\dot{C}(t) &= (1-\alpha)\delta E - h_2 C - r_3 C - \mu C, \qquad (46)\\
\dot{H}(t) &= h_1 I + h_2 C - r_4 H - \mu H,\\
\dot{R}(t) &= (1-\xi) r_1 V_2 + r_1 V_3 + r_2 I + r_3 C + r_4 H - \mu R. \qquad (47)
\end{aligned}$$

In this research, we construct a fractal-fractional model for COVID-19 using the mittag-leffler kernel. This model is described as follows:

$$\begin{aligned}
{}_0^{FFM}D_t^{\varpi,\vartheta} S(t) &= \mu^{\varpi} N^{\varpi} + \Phi^{\varpi} V_1 - \frac{\beta^{\varpi} S(I+C)}{N^{\varpi}} - \Lambda^{\varpi} S\\
&\quad - \mu^{\varpi} S,\\
{}_0^{FFM}D_t^{\varpi,\vartheta} V_1(t) &= \Lambda^{\varpi} S - \Phi^{\varpi} V_1 - \eta^{\varpi} V_1 - \mu^{\varpi} V_1,\\
{}_0^{FFM}D_t^{\varpi,\vartheta} V_2(t) &= \eta^{\varpi} V_1 - \chi^{\varpi} V_2 - (1-\xi^{\varpi}) r_1^{\varpi} V_2 - \mu^{\varpi} V_2,\\
{}_0^{FFM}D_t^{\varpi,\vartheta} V_3(t) &= \chi^{\varpi} V_2 - r_1^{\varpi} V_3 - \mu^{\varpi} V_3,\\
{}_0^{FFM}D_t^{\varpi,\vartheta} E(t) &= \frac{\beta^{\varpi} S(I+C)}{N^{\varpi}} - \delta^{\varpi} E - \mu^{\varpi} E,\\
{}_0^{FFM}D_t^{\varpi,\vartheta} I(t) &= \alpha^{\varpi}\delta^{\varpi} E - h_1^{\varpi} I - r_2^{\varpi} I - \mu^{\varpi} I,\\
{}_0^{FFM}D_t^{\varpi,\vartheta} C(t) &= (1-\alpha^{\varpi})\delta^{\varpi} E - h_2^{\varpi} C - r_3^{\varpi} C - \mu^{\varpi} C,\\
{}_0^{FFM}D_t^{\varpi,\vartheta} H(t) &= h_1^{\varpi} I + h_2^{\varpi} C - r_4^{\varpi} H - \mu^{\varpi} H,\\
{}_0^{FFM}D_t^{\varpi,\vartheta} R(t) &= (1-\xi^{\varpi}) r_1^{\varpi} V_2 + r_1^{\varpi} V_3 + r_2^{\varpi} I + r_3^{\varpi} C\\
&\quad + r_4^{\varpi} H - \mu^{\varpi} R, \qquad (48)
\end{aligned}$$

where $0 < \varpi \leq 1$. The following is the design of the fractional-order PID controller:

$$\begin{aligned}
P_1(t) &= k_p e_1(t) + k_{i0} J_t^{-\chi} e_1(t) + k_{d0}{}^{FFM}D_t^{\varpi,\vartheta} e_1(t),\\
P_2(t) &= k_p e_2(t) + k_{i0} J_t^{-\chi} e_2(t) + k_{d0}{}^{FFM}D_t^{\varpi,\vartheta} e_2(t),\\
P_3(t) &= k_p e_3(t) + k_{i0} J_t^{-\chi} e_3(t) + k_{d0}{}^{FFM}D_t^{\varpi,\vartheta} e_3(t),\\
P_4(t) &= k_p e_4(t) + k_{i0} J_t^{-\chi} e_4(t) + k_{d0}{}^{FFM}D_t^{\varpi,\vartheta} e_4(t),\\
P_5(t) &= k_p e_5(t) + k_{i0} J_t^{-\chi} e_5(t) + k_{d0}{}^{FFM}D_t^{\varpi,\vartheta} e_5(t), \qquad (49)\\
P_6(t) &= k_p e_6(t) + k_{i0} J_t^{-\chi} e_6(t) + k_{d0}{}^{FFM}D_t^{\varpi,\vartheta} e_6(t),\\
P_7(t) &= k_p e_7(t) + k_{i0} J_t^{-\chi} e_7(t) + k_{d0}{}^{FFM}D_t^{\varpi,\vartheta} e_7(t),\\
P_8(t) &= k_p e_8(t) + k_{i0} J_t^{-\chi} e_8(t) + k_{d0}{}^{FFM}D_t^{\varpi,\vartheta} e_8(t),\\
P_9(t) &= k_p e_9(t) + k_{i0} J_t^{-\chi} e_9(t) + k_{d0}{}^{FFM}D_t^{\varpi,\vartheta} e_9(t),
\end{aligned}$$

where $e_1(t) = (S(t) - S^*)$, $e_2(t) = (V_1(t) - V_1^*)$, $e_3(t) = (V_2(t) - V_2^*)$, $e_4(t) = (V_3(t) - V_3^*)$, $a_5(t) = (E(t) - E^*)$, $a_6(t) = (I(t) - I^*)$, $e_7(t) = (C(t) - C^*)$, $e_8(t) = (H(t) - H^*)$, $e_9(t) = (R(t) - R^*)$, k_p, k_i, and k_d are the control gains.

In the system controller eq. (49), the terms $k_p\ e_1(t)$, $k_{i0} J_t^{-\varpi} e_1(t)$, $k_p\ e_2(t)$, $k_{i0} J_t^{-\varpi} e_2(t)$, $k_p\ e_3(t)$, $k_{i0} J_t^{-\varpi} e_3(t)$, $k_p\ e_4(t)$, $k_{i0} J_t^{-\varpi} e_4(t)$, $k_p\ e_5(t)$, $k_{i0} J_t^{-\varpi} e_5(t)$, $k_p\ e_6(t)$, $k_{i0} J_t^{-\varpi} e_6(t)$, $k_p\ e_7(t)$, $k_{i0} J_t^{-\varpi} e_7(t)$, $k_p\ e_8(t)$, $k_{i0} J_t^{-\varpi} e_8(t)$, $k_p\ e_9(t)$, $k_{i0} J_t^{-\varpi} e_9(t)$, $k_{d0}{}^{FFM}D_t^{\varpi,\vartheta} e_1(t)$, $k_{d0}{}^{FFM}D_t^{\varpi,\vartheta} e_2(t)$, $k_{d0}{}^{FFM}D_t^{\varpi,\vartheta} e_3(t)$, $k_{d0}{}^{FFM}D_t^{\varpi,\vartheta} e_4(t)$, $k_{d0}{}^{FFM}D_t^{\varpi,\vartheta} e_5(t)$, $k_{d0}{}^{FFM}D_t^{\varpi,\vartheta} e_6(t)$, $k_{d0}{}^{FFM}D_t^{\varpi,\vartheta} e_7(t)$, $k_{d0}{}^{FFM}D_t^{\varpi,\vartheta} e_8(t)$ and , $k_{d0}{}^{FFM}D_t^{\varpi,\vartheta} e_9(t)$ represent the proportional, integral, and derivative components, respectively. Here, k_p, k_i, and k_d are the corresponding control gains. When $k_i = 0$, the controller eq. (49) becomes a fractional-order PD controller. Similarly, when $k_d = 0$, it reduces to a fractional PI controller. For $\varpi = 1$, the controller eq. (49) functions as a conventional integral-order PID controller.

The following controlled model is obtained by applying controller eq. (49) to model eq. (48):

$$\begin{aligned}
{}_0^{FFM}D_t^{\varpi,\vartheta} S(t) &= \mu^{\varpi} N + \Phi^{\varpi} V_1(t-\tau)\\
&\quad - \frac{\beta^{\varpi} S(t-\tau)(I(t-\tau) + C(t-\tau))}{N^{\varpi}}\\
&\quad - \Lambda^{\varpi} S(t-\tau) - \mu^{\varpi} S(t-\tau) + P_1(t),\\
{}_0^{FFM}D_t^{\varpi,\vartheta} V_1(t) &= \Lambda^{\varpi} S(t-\tau) - \Phi^{\varpi} V_1(t-\tau) - \eta^{\varpi} V_1(t-\tau)\\
&\quad - \mu^{\varpi} V_1(t-\tau) + P_2(t),\\
{}_0^{FFM}D_t^{\varpi,\vartheta} V_2(t) &= \eta^{\varpi} V_1(t-\tau) - \chi^{\varpi} V_2(t-\tau)\\
&\quad - (1-\xi^{\varpi}) r_1^{\varpi} V_2(t-\tau) - \mu^{\varpi} V_2(t-\tau)\\
&\quad + P_3(t),\\
{}_0^{FFM}D_t^{\varpi,\vartheta} V_3(t) &= \chi^{\varpi} V_2(t-\tau) - r_1^{\varpi} V_3(t-\tau)\\
&\quad - \mu^{\varpi} V_3(t-\tau) + P_4(t),\\
{}_0^{FFM}D_t^{\varpi,\vartheta} E(t) &= \frac{\beta^{\varpi} S(t-\tau)(I(t-\tau) + C(t-\tau))}{N^{\varpi}}\\
&\quad - \delta^{\varpi} E(t-\tau) - \mu^{\varpi} E(t-\tau) + P_5(t),\\
{}_0^{FFM}D_t^{\varpi,\vartheta} I(t) &= \alpha^{\varpi}\delta^{\varpi} E(t-\tau) - h_1^{\varpi} I(t-\tau) - r_2^{\varpi} I(t-\tau)\\
&\quad - \mu^{\varpi} I(t-\tau) + P_6(t),\\
{}_0^{FFM}D_t^{\varpi,\vartheta} C(t) &= (1-\alpha^{\varpi})\delta^{\varpi} E(t-\tau) - h_2^{\varpi} C(t-\tau)\\
&\quad - r_3^{\varpi} C(t-\tau) - \mu^{\varpi} C(t-\tau) + P_7(t),\\
{}_0^{FFM}D_t^{\varpi,\vartheta} H(t) &= h_1^{\varpi} I(t-\tau) + h_2^{\varpi} C(t-\tau) - r_4^{\varpi} H(t-\tau)\\
&\quad - \mu^{\varpi} H(t-\tau) + P_8(t),\\
{}_0^{FFM}D_t^{\varpi,\vartheta} R(t) &= (1-\xi^{\varpi}) r_1^{\varpi} V_2(t-\tau) + r_1^{\varpi} V_3(t-\tau)\\
&\quad + r_2^{\varpi} I(t-\tau) + r_3^{\varpi} C(t-\tau)\\
&\quad + r_4^{\varpi} H(t-\tau) - \mu^{\varpi} R(t-\tau) + P_9(t), \qquad (50)
\end{aligned}$$

Added new variables.

$$\begin{aligned}
&\mathcal{P}_1(t) = {}_0J_t^{-\varpi} e_1(t), \mathcal{P}_2(t) = {}_0J_t^{-\varpi} e_2(t), \mathcal{P}_3(t) = {}_0J_t^{-\varpi} e_3(t),\\
&\mathcal{P}_4(t) = {}_0J_t^{-\varpi} e_4(t), \mathcal{P}_5(t) = {}_0J_t^{-\varpi} e_5(t), \mathcal{P}_6(t) = {}_0J_t^{-\varpi} e_6(t),\\
&\mathcal{P}_7(t) = {}_0J_t^{-\varpi} e_7(t), \mathcal{P}_8(t) = {}_0J_t^{-\varpi} e_8(t), \mathcal{P}_9(t) = {}_0J_t^{-\varpi} e_9(t),\\
&{}_0^{FFM}D_t^{\varpi,\vartheta}\mathcal{P}_1(t) = e_1(t), {}_0^{FFM}D_t^{\varpi,\vartheta}\mathcal{P}_2(t) = e_2(t),\\
&{}_0^{FFM}D_t^{\varpi,\vartheta}\mathcal{P}_3(t) = e_3(t), {}_0^{FFM}D_t^{\varpi,\vartheta}\mathcal{P}_4(t) = e_4(t),\\
&{}_0^{FFM}D_t^{\varpi,\vartheta}\mathcal{P}_5(t) = e_5(t), {}_0^{FFM}D_t^{\varpi,\vartheta}\mathcal{P}_6(t) = e_6(t),\\
&{}_0^{FFM}D_t^{\varpi,\vartheta}\mathcal{P}_7(t) = e_7(t), {}_0^{FFM}D_t^{\varpi,\vartheta}\mathcal{P}_8(t) = e_8(t),\\
&{}_0^{FFM}D_t^{\varpi,\vartheta}\mathcal{P}_9(t) = e_9(t).
\end{aligned}$$

Thus, we can express the fractional-order controlled model (50)

as follows:

$$
\begin{aligned}
{}_0^{FFM}D_t^{\varpi,\vartheta}S(t) &= \Big[\mu^{\varpi}N^{\varpi} + \Phi^{\varpi}V_1(t-\tau) - \Lambda^{\varpi}S(t-\tau) \\
&\quad - \frac{\beta^{\varpi}S(t-\tau)\left(I(t-\tau)+C(t-\tau)\right)}{N^{\varpi}} \\
&\quad - \mu^{\varpi}S(t-\tau) + k_p\left(S(t)-S^*\right) \\
&\quad + k_iP_1(t)\Big]\frac{1}{1-k_d}, \\
{}_0^{FFM}D_t^{\varpi,\vartheta}V_1(t) &= \Big[\Lambda^{\varpi}S(t-\tau) - \Phi^{\varpi}V_1(t-\tau) - \eta^{\varpi}V_1\big(t \\
&\quad - \tau\big) - \mu^{\varpi}V_1(t-\tau) + k_p\left(V_1(t)-{V_1}^*\right) \\
&\quad + k_iP_2(t)\Big]\frac{1}{1-k_d}, \\
{}_0^{FFM}D_t^{\varpi,\vartheta}V_2(t) &= \Big[\eta^{\varpi}V_1(t-\tau) - \chi^{\varpi}V_2(t-\tau) \\
&\quad - \left(1-\xi^{\varpi}\right)r_1^{\varpi}V_2(t-\tau) - \mu^{\varpi}V_2(t-\tau) \\
&\quad + k_p\left(V_2(t)-{V_2}^*\right) + k_iP_3(t)\Big]\frac{1}{1-k_d}, \\
{}_0^{FFM}D_t^{\varpi,\vartheta}V_3(t) &= \Big[\chi^{\varpi}V_2(t-\tau) - r_1^{\varpi}V_3(t-\tau) \\
&\quad - \mu^{\varpi}V_3(t-\tau) + k_p\left(V_3(t)-{V_3}^*\right) \qquad (51) \\
&\quad + k_iP_4(t)\Big]\frac{1}{1-k_d}, \\
{}_0^{FFM}D_t^{\varpi,\vartheta}E(t) &= \Big[\frac{\beta^{\varpi}S(t-\tau)\left(I(t-\tau)+C(t-\tau)\right)}{N^{\varpi}} \\
&\quad - \delta^{\varpi}E(t-\tau) - \mu^{\varpi}E(t-\tau) + k_p\big(E(t) \qquad (52) \\
&\quad - E^*\big) + k_iP_5(t)\Big]\frac{1}{1-k_d}, \\
{}_0^{FFM}D_t^{\varpi,\vartheta}I(t) &= \Big[\alpha^{\varpi}\delta^{\varpi}E(t-\tau) - h_1^{\varpi}I(t-\tau) \\
&\quad - r_2^{\varpi}I(t-\tau) - \mu^{\varpi}I(t-\tau) + k_p\big(I(t) \qquad (53) \\
&\quad - I^*\big) + k_iP_6(t)\Big]\frac{1}{1-k_d}, \\
{}_0^{FFM}D_t^{\varpi,\vartheta}C(t) &= \Big[\left(1-\alpha^{\varpi}\right)\delta^{\varpi}E(t-\tau) - h_2^{\varpi}C(t-\tau) \\
&\quad - r_3^{\varpi}C(t-\tau) - \mu^{\varpi}C(t-\tau) + k_p\big(C(t) \\
&\quad - C^*\big) + k_iP_7(t)\Big]\frac{1}{1-k_d}, \\
{}_0^{FFM}D_t^{\varpi,\vartheta}H(t) &= \Big[h_1^{\varpi}I(t-\tau) + h_2^{\varpi}C(t-\tau) - r_4^{\varpi}H\big(t \\
&\quad - \tau\big) - \mu^{\varpi}H\big(t-\tau\big) + k_p\left(H(t)-H^*\right) \\
&\quad + k_iP_8(t)\Big]\frac{1}{1-k_d}, \\
{}_0^{FFM}D_t^{\varpi,\vartheta}R(t) &= \Big[\left(1-\xi^{\varpi}\right)r_1^{\varpi}V_2(t-\tau) + r_1^{\varpi}V_3(t-\tau) \\
&\quad + r_2^{\varpi}I(t-\tau) + r_3^{\varpi}C(t-\tau) + r_4^{\varpi}H(t-\tau) \\
&\quad - \mu^{\varpi}R(t-\tau) + k_p\left(R(t)-R^*\right) \\
&\quad + k_iP_9(t)\Big]\frac{1}{1-k_d}, \\
{}_0^{FFM}D_t^{\varpi,\vartheta}P_1(t) &= \left(S(t)-S^*\right), \\
{}_0^{FFM}D_t^{\varpi,\vartheta}P_2(t) &= \left(V_1(t)-V_2^*\right), \\
{}_0^{FFM}D_t^{\varpi,\vartheta}P_3(t) &= \left(V_2(t)-V_2^*\right), \\
{}_0^{FFM}D_t^{\varpi,\vartheta}P_4(t) &= \left(V_3(t)-V_3^*\right), \\
{}_0^{FFM}D_t^{\varpi,\vartheta}P_5(t) &= \left(E(t)-E^*\right), \\
{}_0^{FFM}D_t^{\varpi,\vartheta}P_6(t) &= \left(I(t)-I^*\right), \\
{}_0^{FFM}D_t^{\varpi,\vartheta}P_7(t) &= \left(C(t)-C^*\right), \\
{}_0^{FFM}D_t^{\varpi,\vartheta}P_8(t) &= \left(H(t)-H^*\right), \\
{}_0^{FFM}D_t^{\varpi,\vartheta}P_9(t) &= \left(R(t)-R^*\right). \qquad (54)
\end{aligned}
$$

The unique positive equilibrium of the controlled system (54) is given by $(S^{\bullet},0)^T$, $(V_1^{\bullet},0)^T$, $(V_2^{\bullet},0)^T$, $(V_3^{\bullet},0)^T$, $(E^{\bullet},0)^T$, $(I^{\bullet},0)^T$, $(C^{\bullet},0)^T$, $(H^{\bullet},0)^T$ and $(R^{\bullet},0)^T$. Notably, the first components of these vectors, $S^{\bullet}$, $V_1^{\bullet}$, $V_2^{\bullet}$, $V_3^{\bullet}$, $E^{\bullet}$, $I^{\bullet}$, $C^{\bullet}$, $H^{\bullet}$ and $R^{\bullet}$, represent the uncontrolled model's singular positive equilibrium eq. (49). Therefore, the unique equilibrium of the model eq. (49) is effectively preserved by the suggested fractional-order PID controller eq. (50).

7. Numerical Scheme

In this section, we solve the following problem

$$
\begin{aligned}
{}_0^{FFM}D_t^{\varpi,\vartheta}z(t) &= q(t,z(t)), \\
z(0) &= z_0.
\end{aligned}
$$

Using the Mittag-Leffler kernel and the new fractional integral, we can convert the previous equation into

$$
\begin{aligned}
z(t) &= z(0) + \frac{1-\varpi}{\mathcal{AB}(\varpi)}t^{1-\vartheta}q(t,z(t)) \\
&\quad + \frac{\varpi}{\mathcal{AB}(\varpi)\Gamma(\varpi)}\int_0^t q(\varsigma,z(\varsigma))(t-\varsigma)^{\varpi-1}\varsigma^{1-\vartheta}d\varsigma.
\end{aligned}
$$

At point $t_{k+1} = (k+1)\Delta t$, we get

$$
\begin{aligned}
z(t_{k+1}) &= z(0) + \frac{1-\varpi}{\mathcal{AB}(\varpi)}t_k^{1-\vartheta}q(t_k,z(t_k)) \\
&\quad + \frac{\varpi}{\mathcal{AB}(\varpi)\Gamma(\varpi)}\int_0^{t_{k+1}} q(\varsigma,z(\varsigma))(t_{k+1}-\varsigma)^{\varpi-1}\varsigma^{1-\vartheta}d\varsigma.
\end{aligned}
$$

For simplicity, we shall take as

$$
\mathcal{Q}(t,z(t)) = q(\varsigma,z(\varsigma))\varsigma^{1-\vartheta}.
$$

Additionally, we have

$$z\left(t_{k+1}\right)=z\left(0\right)+\frac{1-\varpi}{\mathcal{AB}\left(\varpi\right)}\mathcal{Q}\left(t_k,z\left(t_k\right)\right)+\frac{\varpi}{\mathcal{AB}\left(\varpi\right)\Gamma\left(\varpi\right)}\sum_{\nu=2}^{k}\int_{t_\nu}^{t_{\nu+1}}\mathcal{Q}\left(\varsigma,z\left(\varsigma\right)\right)\left(t_{k+1}-\varsigma\right)^{\varpi-1}\varsigma^{1-\vartheta}d\varsigma. \tag{55}$$

We put the Newton polynomial into eq. (55) as we did earlier. After that, the equation above can be arranged as follows:

$$\begin{aligned}z^{k+1}=&\,z\left(0\right)+\frac{1-\varpi}{\mathcal{AB}\left(\varpi\right)}\mathcal{Q}\left(t_k,z\left(t_k\right)\right)\\&+\frac{\varpi}{\mathcal{AB}\left(\varpi\right)\Gamma\left(\varpi\right)}\sum_{\nu=2}^{k}\mathcal{Q}\left(t_{\nu-2},z^{\nu-2}\right)\Delta\int_{t_\nu}^{t_{\nu+1}}\left(t_{k+1}-\varsigma\right)^{\varpi-1}d\varsigma+\frac{\varpi}{\mathcal{AB}\left(\varpi\right)\Gamma\left(\varpi\right)}\sum_{\nu=2}^{k}\frac{\mathcal{Q}\left(t_{\nu-1},z^{\nu-1}\right)}{\Delta t}\\&-\frac{\mathcal{Q}\left(t_{\nu-2},z^{\nu-2}\right)}{\Delta t}\int_{t_\nu}^{t_{\nu+1}}\left(\varsigma-t_{\nu-2}\right)\left(t_{k+1}-\varsigma\right)^{\varpi-1}d\varsigma\\&+\frac{\varpi}{\mathcal{AB}\left(\varpi\right)\Gamma\left(\varpi\right)}\sum_{\nu=2}^{k}\frac{\mathcal{Q}\left(t_\nu,z^{\nu}\right)}{2(\Delta t)^2}-\frac{2\mathcal{Q}\left(t_{\nu-1},z^{\nu-1}\right)}{2(\Delta t)^2}\\&+\frac{\mathcal{Q}\left(t_{\nu-2},z^{\nu-2}\right)}{2(\Delta t)^2}\int_{t_\nu}^{t_{\nu+1}}\left(\varsigma-t_{\nu-2}\right)\left(\varsigma-t_{\nu-1}\right)\left(t_{k+1}-\varsigma\right)^{\varpi-1}d\varsigma.\end{aligned} \tag{56}$$

We can compute the integrals in eq. (56) in the following ways

$$\begin{aligned}\int_{t_\nu}^{t_{\nu+1}}\left(t_{k+1}-\varsigma\right)^{\varpi-1}d\varsigma&=\frac{(\Delta t)^{\varpi}}{\varpi}\left[\left(k-\nu+1\right)^{\varpi}-\left(k-\nu\right)^{\varpi}\right],\\\int_{t_\nu}^{t_{\nu+1}}\left(\varsigma-t_{\nu-2}\right)\left(t_{k+1}-\varsigma\right)^{\varpi-1}d\varsigma&=\frac{(\Delta t)^{\varpi+1}}{\varpi(\varpi+1)}\left[\left(k-\nu+1\right)^{\varpi}\left(k-\nu+3+2\varpi\right)-\left(k-\nu\right)^{\varpi}\left(k-\nu+3+3\varpi\right)\right],\\\int_{t_\nu}^{t_{\nu+1}}\left(\varsigma-t_{\nu-2}\right)\left(\varsigma-t_{\nu-1}\right)\left(t_{k+1}-\varsigma\right)^{\varpi-1}d\varsigma&=\frac{(\Delta t)^{\varpi+2}}{\varpi\left(\varpi+1\right)\left(\varpi+2\right)}\begin{bmatrix}\Psi_7\\\Psi_8\end{bmatrix},\end{aligned}$$

where

$$\begin{aligned}\Psi_7=&\left(k-\nu+1\right)^{\varpi}\left[2(k-\nu)^2+(3\varpi+10)\left(k-\nu\right)+2\varpi^2+9\varpi+12\right],\\\Psi_8=&-\left(k-\nu\right)^{\varpi}\left[2(k-\nu)^2+(5\varpi+10)\left(k-\nu\right)+6\varpi^2+18\varpi+12\right].\end{aligned}$$

Putting them into the eq. (56) and changing $\mathcal{Q}\left(t,z\left(t\right)\right)=q\left(\varsigma,z\left(\varsigma\right)\right)\varsigma^{1-\vartheta}$, numerical strategy that follows can be obtained

$$\begin{aligned}z^{k+1}=&\,z\left(0\right)+\frac{1-\varpi}{AB\left(\varpi\right)}t_k^{1-\vartheta}q\left(t_k,z\left(t_k\right)\right)+\frac{\varpi(\Delta t)^{\varpi}}{AB\left(\varpi\right)\Gamma\left(\varpi+1\right)}\\&\times\sum_{\nu=2}^{k}t_{\nu-2}^{1-\vartheta}q\left(t_{\nu-2},z^{\nu-2}\right)\begin{bmatrix}\left(k-\nu+1\right)^{\varpi}\\-\left(k-\nu\right)^{\varpi}\end{bmatrix}\\&+\frac{\varpi(\Delta t)^{\varpi}}{AB\left(\varpi\right)\Gamma\left(\varpi+2\right)}\sum_{\nu=2}^{k}t_{\nu-1}^{1-\vartheta}q\left(t_{\nu-1},z^{\nu-1}\right)\\&-qt_{\nu-2}^{1-\vartheta}\left(t_{\nu-2},z^{\nu-2}\right)\begin{bmatrix}\left(k-\nu+1\right)^{\varpi}\left(k-\nu+3+2\varpi\right)\\-\left(k-\nu\right)^{\varpi}\left(k-\nu+3+3\varpi\right)\end{bmatrix}\\&+\frac{\varpi\left(\Delta t\right)^{\varpi}}{2AB\left(\varpi\right)\Gamma\left(\varpi+3\right)}\sum_{\nu=2}^{k}t_{\nu}^{1-\vartheta}q\left(t_\nu,z^{\nu}\right)\\&-2t_{\nu-1}^{1-\vartheta}q\left(t_{\nu-1},z^{\nu-1}\right)+qt_{\nu-2}^{1-\vartheta}\left(t_{\nu-2},z^{\nu-2}\right)\\&\times\begin{bmatrix}\Psi_9\\\Psi_{10}\end{bmatrix},\\\Psi_9=&\left(k-\nu+1\right)^{\varpi}\left[2(k-\nu)^2+(3\varpi+10)\left(k-\nu\right)+2\varpi^2+9\varpi+12\right],\\\Psi_{10}=&-\left(k-\nu\right)^{\varpi}\left[2(k-\nu)^2+(5\varpi+10)\left(k-\nu\right)+6\varpi^2+18\varpi+12\right].\end{aligned}$$

The flowchart shown in Figure 4 represents a complete scenario for the numerical technique used in this paper.

8. Results of Proposed Scheme

The analyzed COVID-19 model's graphical findings are shown in this section. The initial conditions and parameter values can be analyzed in [4]. Figures 5 to 13 demonstrate the impact of fractal dimension ϑ and fractional order ϖ, respectively. In Figure 5a susceptible individuals decrease as time progresses. Low fractional orders ϖ cause the decrease to be faster and higher fractional order, slower. In Figure 5b, the curves for different fractional orders are more evident and this is attributable to increasing effect of fractional dynamics at a certain fractal dimension ϑ. Higher fractional orders represent a faster vaccine update, that is more people are getting vaccinated and earlier as shown in Figure 6a. The growth of vaccination in Figure 6b, on the other hand, is slower than in Figure 6a because of differing population features. The graph shows a more gradual increase, with a larger impact of fractional orders on the speed of vaccination. Higher fractional orders Figure 7a result in a more rapid increase in second dose vaccinations. The rise in second dose vaccination Figure 7b is slower compared to Figure 7a, reflecting the effect of the reduced fractal dimension. This could indicate longer intervals between doses or a slower overall vaccination campaign. The increase is slower Figure 8a than for the first and second doses, with higher fractional orders leading to faster uptake. The third dose in Figure 8b uptake is even slower here, showing the impact of both fractional dynamics and the fractal dimension on booster administration. The exposure dynamics are more prolonged, with slower transitions compared to Figure 9a illustrating a slower transmission across a racially/ethnically homogenous population. The infection peaks and falls off in Figure 10a, where the fractional order has a pronounced Peaking effect on this peak time of catch. Under this dimension Fig-

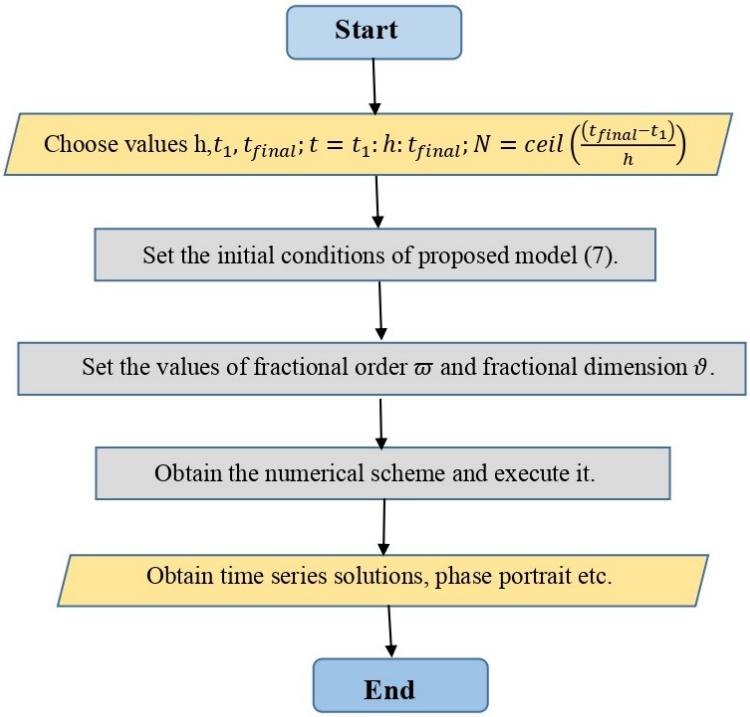

Figure 4. The proposed work flowchart.

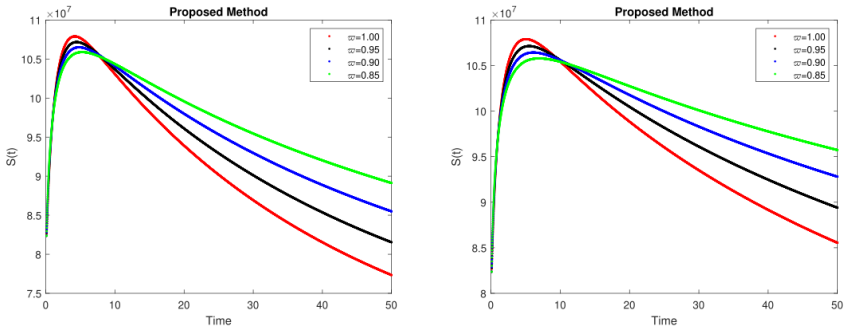

(a) $\vartheta = 0.9$ **(b)** $\vartheta = 0.8$

Figure 5. Simulation of S(t) at different fractional values and dimension

ure 10b, the infection curve spreads out more, with a lower peak and slower decline signifying an extended wave of epidemic. The infection peak and its descending effects both have fractional orders in Figure 11a, which may indicate delayed or chronic influences. Figure Figure 11b similar to Figure 11a, but the peak is lower and spread over a longer period, again reflecting slower dynamics in a more complex spatial environment. The number of isolated individuals in Figure 12a increases initially as more people are infected, with a peak that is influenced by the fractional orders. The isolation numbers peak later and decline more slowly Figure 12b, indicating prolonged periods of isolation under a lower fractal dimension. Higher fractional orders tend to result in quicker recoveries Figure 13a, reflecting a faster resolution of the epidemic. Recovery is slower, with the influence of fractional orders more pronounced, indicating a more prolonged epidemic with slower recovery rates Figure 13b. The use of fractional orders and fractal dimensions allows for a more nuanced understanding of the spread and control of COVID-19 by incorporating memory effects and spatial heterogeneity.

9. Conclusion

Many serious illnesses have recently surfaced in various parts of the world. In this paper, we have forecast future trends in the global COVID-19 epidemic using a mathematical model constructed with a fractal fractional Atangana Baleanu Caputo (ABC) type operator. To study the outbreak dynamics, we carried out both qualitative and quantitative investigations. The qualitative analysis covered the existence, uniqueness, and stability of solutions, while the quantitative part involved extensive numerical simulations. In particular, the Ulam–Hyres stability of the COVID-19 model was demonstrated, ensuring the model's robustness under small perturbations. Furthermore, we

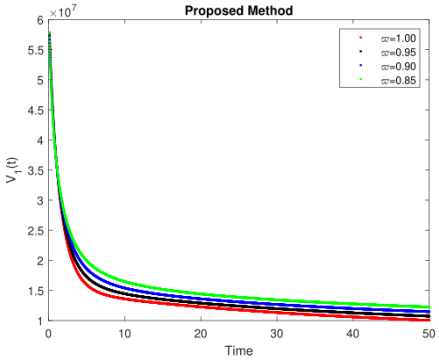

(a) $\vartheta = 0.9$

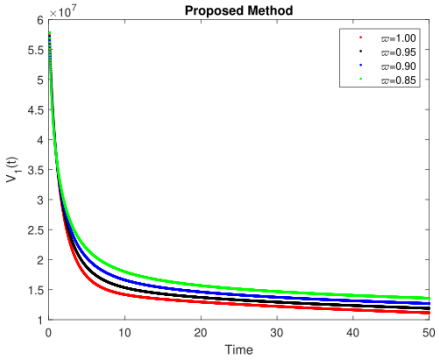

(b) $\vartheta = 0.8$

Figure 6. Simulation of $V_1(t)$ at different fractional values and dimension

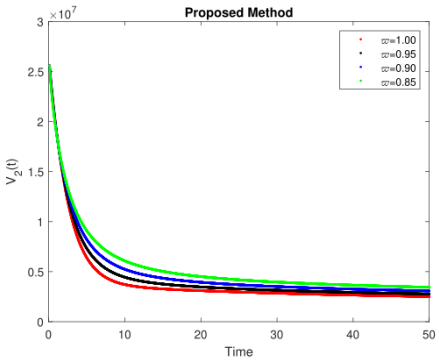

(a) $\vartheta = 0.9$

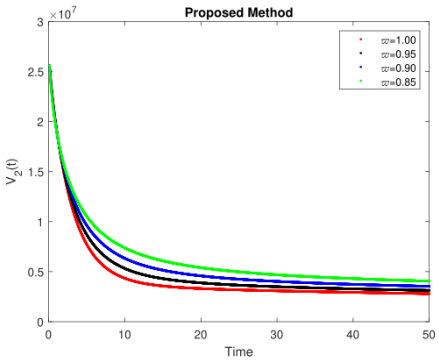

(b) $\vartheta = 0.8$

Figure 7. Simulation of $V_2(t)$ at different fractional values and dimension

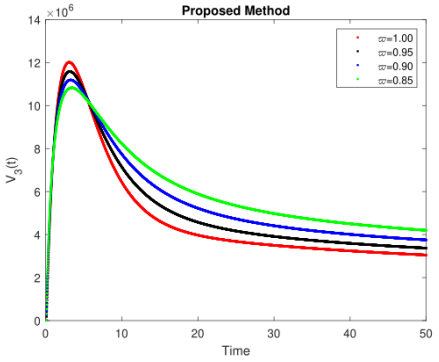

(a) $\vartheta = 0.9$

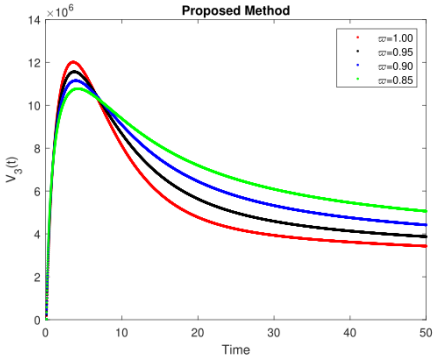

(b) $\vartheta = 0.8$

Figure 8. Simulation of $V_3(t)$ at different fractional values and dimension

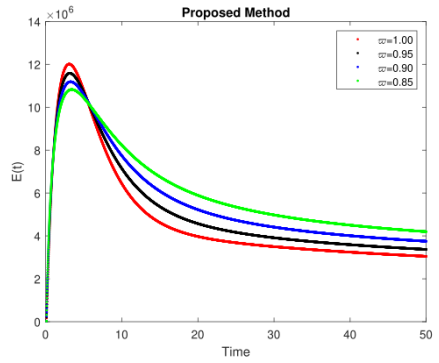

(a) $\vartheta = 0.9$

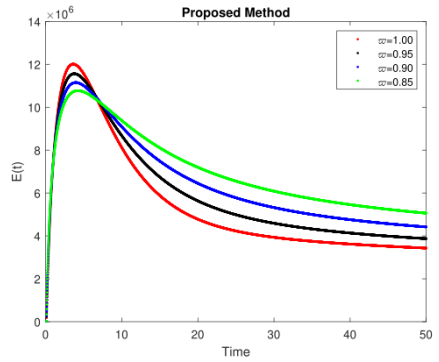

(b) $\vartheta = 0.8$

Figure 9. Simulation of E(t) at different fractional values and dimension

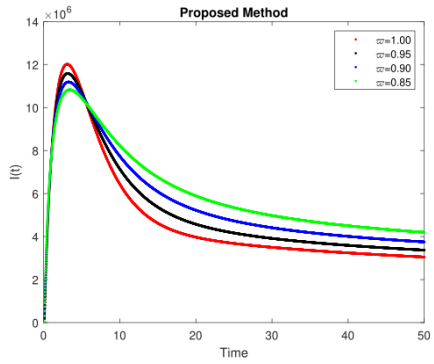

(a) $\vartheta = 0.9$

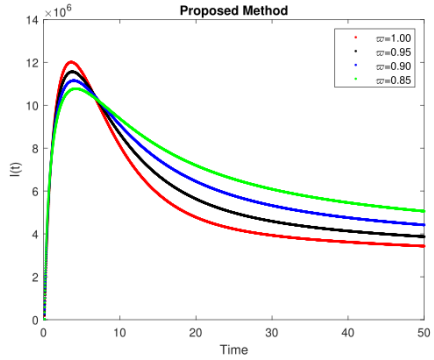

(b) $\vartheta = 0.8$

Figure 10. Simulation of I(t) at different fractional values and dimension

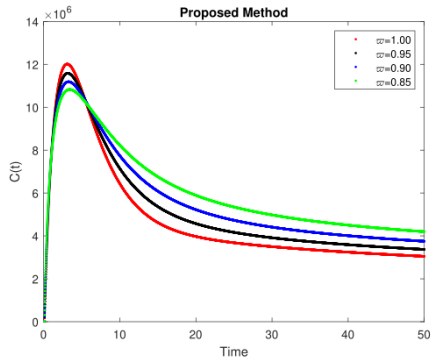

(a) $\vartheta = 0.9$

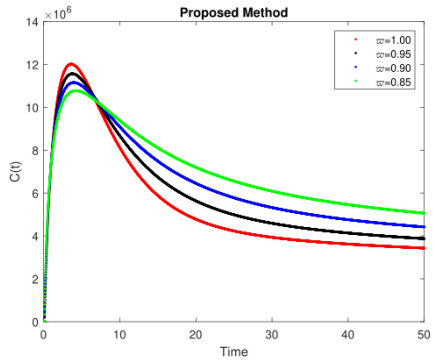

(b) $\vartheta = 0.8$

Figure 11. Simulation of C(t) at different fractional values and dimension

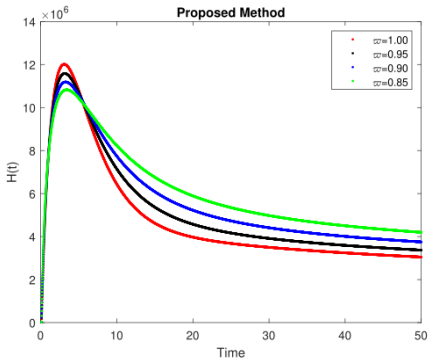

(a) $\vartheta = 0.9$

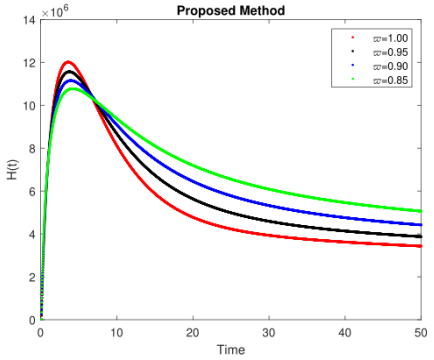

(b) $\vartheta = 0.8$

Figure 12. Simulation of H(t) at different fractional values and dimension

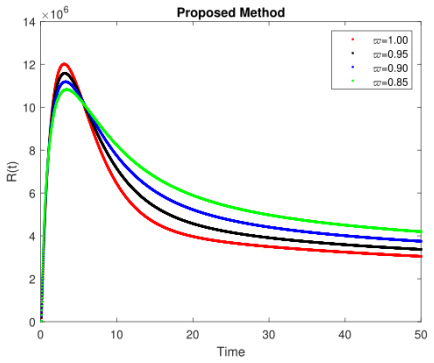

(a) $\vartheta = 0.9$

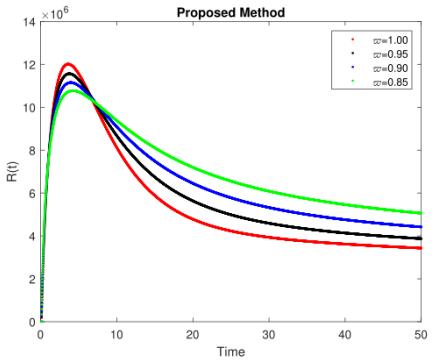

(b) $\vartheta = 0.8$

Figure 13. Simulation of R(t) at different fractional values and dimension

examined how PID-based control strategies enhance the suppression of disease transmission within a fractional modeling framework, revealing that the inclusion of fractional and fractal ordering provides richer memory effects and more accurate dynamic responses.

Our findings highlight that the proposed approach is highly beneficial for planning, decision- making, and implementing effective control interventions such as mask use, social distancing, and vaccination. The results also align with recent studies emphasizing the role of memory- dependent operators in capturing real-world epidemic dynamics more accurately [19, 20]. In future research, heterogeneity may be incorporated using reaction diffusion systems to better reflect spatial spread, while stochasticity and time delay elements could capture uncertainties and behavioral changes over time [21, 22]. Moreover, integrating multiple co-circulating COVID-19 variants and comorbidities into the model together with additional control variables such as age structured vaccination or antiviral treatment could deepen our understanding of epidemic interactions and improve predictive capability [23, 24]. Such extensions would not only broaden the theoretical framework but also enhance its practical usefulness in guiding public health strategies.

Author Contributions. **Farman, M.**: Conceptualization, methodology, and writing original draft preparation. **Alfiniyah, C.**: Validation, Formal analysis, and writing original draft preparation. **Fatmawati**: Investigation, writing review and editing. **Rois, M. A.**: Software, and investigation. **Jamil, K.**: Formal analysis, investigation, visualization, and project administration.

Acknowledgement. The authors are thankful the editors and reviewers who have supported us in improving this manuscript.

Funding. This research received no external funding.

Conflict of interest. The authors declare no conflict of interest.

Data availability. Not applicable.

References

[1] Worldometers"Indonesia COVID - Coronavirus Statistics," https://www.worldometers.info/coronavirus/, 2021, Accessed on 15 April 2021.

[2] WHO, "Pertimbangan-pertimbangan untuk karantina individu dalam konteks penanggulangan penyakit coronavirus (COVID-19)," 2020.

[3] M. Coccia, "Improving preparedness for next pandemics: Max level of COVID-19 vaccinations without social impositions to design effective health policy and avoid flawed democracies," *Environmental research*, vol. 13, p. 113566, 2022. DOI:10.1016/j.envres.2022.113566

[4] M. A. Rois, Fatmawati, and C. Alfiniyah, "Two isolation treatments on the COVID-19 model and optimal control with public education," *Jambura Journal of Biomathematics (JJBM)*, vol. 4, no. 1, pp. 88–94, 2023. DOI:10.34312/jjbm.v4i1.19963

[5] M. A. Rois *et al.*, "Modeling and optimal control of COVID-19 with comorbidity and three-dose vaccination in Indonesia," *Journal of Biosafety and Biosecurity*, vol. 6, no. 3, pp. 181–195, 2024. DOI:10.1016/j.jobb.2024.06.004

[6] M. Caputo and M. Fabrizio, "A new definition of fractional derivative without singular kernel," *Progress in Fractional Differentiation & Applications*, vol. 1, no. 2, pp. 73–85, 2015.

[7] J. Losada and J. J. Nieto, "Properties of a new fractional derivative without singular kernel,". *Progr. Fract. Differ. Appl.*, vol. 1, no. 2, pp. 87–92, 2015.

[8] A. Atangana and B. S. T. Alkahtani, "Analysis of the Keller Segel model with a fractional derivative without singular kernel," *Entropy*, vol. 17, no. 6, pp. 4439–4453, 2015. DOI:10.3390/e17064439

[9] M. Farman *et al.*, "A control of glucose level in insulin therapies for the development of artificial pancreas by Atangana Baleanu derivative,". *Alexandria Engineering Journal*, vol. 59, no. 4, pp. 2639–2648, 2020. DOI:10.1016/j.aej.2020.04.027

[10] M. Toufik and A. Atangana, "New numerical approximation of fractional derivative with non-local and non-singular kernel: application to chaotic models," *The european physical journal plus*, vol. 132, pp. 1–16, 2017. DOI:10.1140/epjp/i2017-11717-0

[11] M. A. Khan *et al.*, "The dynamics of COVID-19 with quarantined and isolation," *Advances in Difference Equations*, vol. 2020, no. 1, p. 425, 2020. DOI:10.1186/s13662-020-02882-9

[12] E. M. Abd-Elaziz, M. Marin, and M. I. Othman, "On the effect of Thomson and initial stress in a thermo-porous elastic solid under GN electromagnetic theory," *Symmetry*, vol. 11, no. 3, p. 413, 2019. DOI:10.3390/sym11030413

[13] S. Jamil *et al.*, "Stability and complex dynamical analysis of COVID-19 epidemic model with non-singular kernel of Mittag-Leffler law," *Journal of Applied Mathematics and Computing*, vol. 70, pp. 3441–3476, 2024. DOI:10.1007/s12190-024-02105-4

[14] M. Farman *et al.*, "Numerical study and dynamics analysis of diabetes mellitus with co-infection of COVID-19 virus by using fractal fractional operator," *Scientific Reports*, vol. 14, no. 1, p. 16489, 2024. DOI:10.1038/s41598-024-60168-6

[15] P. A. Naik *et al.*, "Analysis and modeling with fractal-fractional operator for an epidemic model with reference to COVID-19 modeling," *Partial Differential Equations in Applied Mathematics*, vol. 10, p. 100663, 2024. DOI:10.1016/j.padiff.2024.100663

[16] K. S. Nisar *et al.*, "A review of fractional order epidemic models for life sciences problems: Past, present and future," *Alexandria Engineering Journal*, vol. 95, pp. 283–305, 2024. DOI:10.1016/j.aej.2024.03.059

[17] M. Farman and C. Alfiniyah, "A constant proportional caputo operator for modeling childhood disease epidemics," *Decision Analytics Journal*, vol. 10, p. 100393, 2024. DOI:10.1016/j.dajour.2023.100393

[18] A. Atangana, "Fractal-fractional differentiation and integration: connecting fractal calculus and fractional calculus to predict complex system," *Chaos, solitons & fractals*, vol. 102, pp. 396–406, 2017. DOI:10.1016/j.chaos.2017.04.027

[19] A. Atangana and D. Baleanu, "New fractional derivatives with nonlocal and non-singular kernel: Theory and application to heat transfer model," *Thermal Science*, vol. 20, no. 2, pp. 763–769, 2016. DOI:10.2298/TSCI160111018A

[20] L. C. D. Barros *et al.*, "The memory effect on fractional calculus: an application in the spread of COVID-19," *Comp. Appl. Math.*, vol. 40, no. 3, p. 72, 2021. DOI:10.1007/s40314-021-01456-z

[21] R. Zarin and U. W. Humphries, "Modeling the dynamics of COVID-19 Epidemic with a reaction-diffusion framework: a case study from Thailand," *Eur. Phys. J. Plus*, vol. 139, p. 1076, 2024. DOI:10.1140/epjp/s13360-024-05870-0

[22] W. Wu *et al.*, "The effect of time delay on the dynamics of a fractional-order epidemic model," *Adv Cont Discr Mod*, vol. 9, pp. 1–33, 2025. DOI:10.1186/s13662-025-03868-1

[23] J. Ssebuliba *et al.*, "Mathematical modelling of COVID-19 transmission dynamics in a partially comorbid community," *Partial Differential Equations in Applied Mathematics*, vol. 5, p. 100212, 2022. DOI:10.1016/j.padiff.2021.100212

[24] V. Ambalarajan *et al.*, "Multi-strain COVID-19 dynamics with vaccination strategies: Mathematical modeling and case study," *Alexandria Engineering Journal*, vol. 119, pp. 665-684, 2025. DOI:10.1016/j.aej.2025.01.105.